



1 **Transferability of machine learning-based modeling frameworks across flood events**
2 **for hindcasting maximum river flood depths in coastal watersheds**

3 Maryam Pakdehi^{1,2}, Ebrahim Ahmadisharaf^{1,2*}, Behzad Nazari³, Eunsaeem Cho^{1,2}

4
5 ¹Department of Civil and Environmental Engineering, FAMU-FSU College of Engineering,
6 Tallahassee, FL 32310

7 ²Resilient Infrastructure and Disaster Response Center, FAMU-FSU College of Engineering,
8 Tallahassee, FL 32310

9 ³Department of Civil Engineering, University of Texas at Arlington, Arlington, TX 76010

10

11 ***Corresponding Author:**

12 Dr. Ebrahim Ahmadisharaf

13 Research Faculty I

14 Department of Civil and Environmental Engineering

15 Resilient Infrastructure and Disaster Response Center

16 FAMU-FSU College of Engineering

17 Tallahassee, FL 32310, USA

18 Tel: +1 716-803-5498

19 Emails: eahmadisharaf@eng.famu.fsu.edu and eascesharif@gmail.com



20 **Abstract**

21 Despite applications of machine learning (ML) models for predicting floods, their transferability
22 for out-of-sample data has not been explored. This paper developed an ML-based model for
23 hindcasting maximum flood depths during major events in coastal watersheds and evaluated its
24 transferability across other events (out-of-sample). The model considered spatial distribution of
25 influential factors, which explain underlying physical processes, to hindcast maximum river flood
26 depths. Our model evaluation in a HUC6 watershed in Northeastern US showed that the model
27 satisfactorily hindcasted maximum flood depths at 116 stream gauges during a major flood event,
28 Hurricane Ida (R^2 of 0.92). The pre-trained, validated model was successfully transferred to three
29 other major flood events, Hurricanes Isaias, Sandy, and Irene ($R^2 > 0.71$). Our results showed that
30 ML-based models can be transferable for hindcasting maximum river flood depths across events
31 when informed by the spatial distribution of pertinent features and underlying physical processes
32 in coastal watersheds.

33 **Keywords**

34 Flood hindcasting; Machine learning algorithms; Maximum flood depth; Model transferability;
35 Coastal watersheds.

36 **1. Introduction**

37 Floods can damage civil infrastructure, business disruptions, and environmental degradation.
38 Nonstationary factors, including land use changes, population growth, and global warming, can
39 exacerbate the risk of flood events (Davenport, Burke, and Diffenbaugh 2021; National Academies
40 of Sciences, Engineering, and Medicine 2019; Galloway et al. 2018). For instance, (Galloway et
41 al. 2018) projected that changes in climate cause a 26.4% increase in the United States flood risks
42 by 2050. This increase in flood risk is expected to disproportionately affect poor communities,



43 leading to job losses and displacement of residents (Hino and Nance 2021). Therefore, effective
44 adaptation and mitigation strategies are urgently needed to maintain resilience against extreme
45 future floods (Hemmati et al. 2020; Qi et al. 2021; Wing et al. 2022).

46 To propose effective protection strategies, predictive models are used to evaluate watershed
47 responses under various plausible flood scenarios (Fernández-Pato et al. 2016; Kundzewicz et al.
48 2019; Viglione et al. 2014). These models are essential tools to inform decision makers about
49 suitable risk management strategies and actions. Flood models can be broadly categorized as
50 physically-based, morphologic-based and data-driven.

51 Physically-based models, widely used for predicting hydrologic events, are considered
52 reliable tools for assessing different flood scenarios (Fernández-Pato et al. 2016). These models
53 solve the shallow water equations to derive flood characteristics. Developing physically-based
54 models require certain meteorologic, hydrologic, and geomorphologic data. If these data are not
55 available at the desired scale, such models cannot be developed. For instance, global inundation
56 models are available across the globe, but they may not be efficient for small scale applications.
57 In such instances, data-driven models can be a flexible alternative as they can adapt to varying
58 levels of data availability by focusing on the features with sufficient data. This flexibility remains
59 one of the advantages of data-driven models over strictly data-dependent physically-based models.
60 Physically-based models also need significant computational resources, especially in the case of
61 high-resolution, multidimensional (2D and 3D) or stochastic models that necessitate numerous
62 simulations. To enhance the speed of flood simulations, techniques such as parallel computing,
63 graphics processing units (GPUs), and simplified models have been utilized (Costabile, Costanzo,
64 and Macchione 2017; Kalyanapu et al. 2011; Ming et al. 2020; Sridhar, Ali, and Sample 2021;



65 Zahura et al. 2020). However, resources for utilizing these approaches are not always available
66 (Zhang et al. 2014).

67 Morphologic-based models, which approximate flat-water surfaces over small spatial scales,
68 are also used for flood predictions (Bates 2022). Bathtub (Anderson et al. 2018; Kulp & Strauss
69 2019) and height above nearest drainage (HAND; Rennó et al. 2008) are two widely used models
70 in this modeling category. Jafarzadegan and Merwade (2019) used a probabilistic function based
71 on HAND, computed from a digital elevation model (DEM), and optimized it for accuracy, to
72 delineate 100-year floodplains. (Zheng et al. 2018) developed a synthetic rating curve using the
73 HAND method, which accurately represents the river shape and water level measurements, like
74 hydraulic models or stream gauge readings. While these models are computationally efficient, they
75 can overestimate flooded area and are limited to the number of features they use; these models rely
76 on topographic data (Bates 2022; Bates et al. 2005) and tend only to work well in confined valleys.
77 The sole use of topographic data makes HAND-based models impractical for low-lying areas,
78 especially coastal watersheds that experience a combination of hydrologic and oceanic processes
79 (tidal influences, storm surges and wave action); other flood influencing factors, which represent
80 such overlooked underlying physical processes, are needed along fore predictions in such
81 watersheds. Coastal regions experience a combination of oceanic and hydrological processes,
82 which might not be fully represented by HAND. Additionally, both HAND-based and bathtub
83 models are limited in representing such terrains as they might not fully capture the intricate
84 interactions between oceanic and hydrologic factors in coastal areas. Consequently, in coastal
85 watersheds, where unconfined floodplains and complex interactions are prevalent, alternative
86 modeling approaches that consider a broader range of factors are crucial for producing reliable



87 flood predictions. Incorporating these overlooked underlying physical processes becomes essential
88 in providing comprehensive flood predictions in these intricate environments.

89 Machine learning (ML) and deep learning (DL) models offer an alternative approach that can
90 rapidly capture complex relationships between various influencing factors and flood
91 characteristics. ML models have the potential to provide satisfactory predictions, making them a
92 valuable tool for improving flood prediction accuracy (Mishra et al. 2022). Such data-driven
93 models have gained popularity in overcoming the limitations of physically-based and
94 morphologic-based models in flood analyses (Khosravi et al. 2018). These models mathematically
95 represent the nonlinearity of flood dynamics using pertinent features and observed flood data, and
96 through their intricate nonlinear structures and algorithms. Data-driven models have been found
97 as promising tools due to their quick development time and minimal input requirements (Guo et
98 al. 2021; Löwe et al. 2021; Zahura et al. 2020); therefore, they are effective for short-term forecasts
99 and nowcasts (Mosavi, Ozturk, and Chau 2018). ML and DL models can discover and leverage
100 hidden patterns within the data, leading to improved performance as the amount of available data
101 increases. By recognizing and utilizing these underlying patterns inherent in the data, ML and DL
102 models can make satisfactory predictions (in terms of minimum error in estimating flood
103 characteristics like depth) and generate valuable insights. Example data-driven models for flood
104 prediction include multi-criteria decision-making techniques, multiple linear regression, artificial
105 neural networks (ANNs), random forest, convolutional neural networks, support vector machine,
106 support vector regression, frequency ratio models, and weights-of-evidence models (Adamowski
107 et al. 2011; Kim et al. 2016; Rafei-Sardooi et al. 2021; Rahmati et al. 2016; Rezaie et al. 2022;
108 Wang et al. 2015; Youssef et al. 2022).



109 Previous research has shown that various ML algorithms are effective in predicting flood
110 extents and generating susceptibility maps, with a focus on classification ML models (Khosravi et
111 al. 2018; Rahmati et al. 2016; Rezaie et al. 2022; Youssef et al. 2022). However, these studies may
112 have limitations in terms of their experimental design and scope. For instance, some of these
113 studies created simplified datasets of flooded and unflooded points using remote sensing. The
114 datasets were often split into training and validation data, and different ML models were examined
115 on the same dataset. Another limitation of these ML studies is the reliance on a single event for
116 training and validation. These limitations call for studies that evaluate more complex
117 methodologies and a broader range of scenarios on the effectiveness of ML algorithms for
118 predicting flood characteristics.

119 Another application of ML models for flood inundation prediction has been incorporating them
120 with physically-based models for improving their performance. Such applications are based on the
121 hybrid use of ML and physically-based modeling categories. For instance, Chang et al. (2022)
122 suggested an approach that incorporated principal component analysis, self-organizing maps, and
123 nonlinear autoregressive models with exogenous inputs to mine spatiotemporal data and forecast
124 regional flood inundation. They recognized the value of using ML algorithms in conjunction with
125 a 2D hydraulic model to simulate urban flood inundation while taking different rainfall
126 occurrences into account. Elkharchy (2022) developed a hybrid approach to predict flash flood
127 depths combining 2D hydraulic modeling with ML; water depths simulated by the Hydrologic
128 Engineering Center's River Analysis System (HEC-RAS; Brunner 2016) model served as inputs
129 to ML algorithms. Löwe et al. (2021) trained an ANN model to identify patterns in rainfall
130 hyetographs and topographic data to enable fast predictions of flood depths for new rain events
131 and locations (out of training sample data) complemented by 2D hydrodynamic simulations. Guo



132 et al. (2021) used a convolutional neural network model trained on flood simulation patch data
133 from the CADDIES cellular-automata model to perform image-to-image translation for rapid
134 urban flood prediction and risk assessment. To effectively simulate maximum flood extent and
135 depth, Hosseiny et al. (2020) created a system that combines a hydraulic model with ML
136 algorithms. Zahura et al. (2020) used simulations from high-resolution 1D/2D physically-based
137 models as training and test data for a random forest model that included topographic and
138 environmental characteristics to estimate hourly water depths. In these applications, flood depth,
139 which is important for risk assessments and damage estimates (Merz et al. 2010), has been
140 predicted by coupling physically-based and ML models. These coupled modeling studies
141 demonstrated the complimentary benefits of physically-based models along with ML algorithms
142 in producing flood modeling outputs, but the computational expense is still an application barrier.
143 Another significant challenge inherent in these studies lies in their dependence on 2D models for
144 training purposes. Furthermore, there appears to be a gap in demonstrating the ability of these
145 studies to successfully predict outcomes beyond their training samples. For instance, we are
146 unaware of studies that convincingly exhibit the capability of ML models to predict events of
147 greater magnitude than those utilized in their training datasets.

148 Despite previous efforts, the development of computationally efficient and user-friendly flood
149 prediction models remains a challenge. ML-based models, although promising and
150 computationally efficient, have not gained widespread acceptance among practitioners due to
151 concerns about their reliance on predicting flood characteristics for other events (out-of-sample).
152 While some studies have demonstrated promising results in generating flood hazard maps by
153 applying models to new geographical areas not used for training (Bentivoglio et al. 2022; Kratzert
154 et al. 2019; Zhao et al. 2021), few studies have examined the transferability of coupled ML and



155 physically-based models for predicting flood depths by applying them to unseen data not used in
156 training (Guo et al. 2021; Löwe et al. 2021). It, therefore, remains unclear whether an ML-based
157 model, which is trained, validated, and tested against a historical event, performs satisfactorily in
158 predicting flood characteristics of other events in the same watershed. Floods originate from
159 various sources, especially in coastal areas, where flooding heavily relies on the unique
160 characteristics of storm events. High wind events tend to generate storm surges that move
161 upstream, while intense rainfall over upstream watersheds leads to fluvial flooding that moves
162 downstream towards the coast. Conversely, slow-moving storm systems can cause intense local
163 rainfall, resulting in overland runoff entering rivers along their paths rather than a concentrated
164 upstream inflow flood wave. Hence, it is crucial to avoid overfitting an ML model to a single
165 historical flood event, as it can lead to significant underperformance in handling other events.

166 A further limitation of past research is the sole focus on predicting greatest flood extents using
167 classification-based algorithms, while the performance of regression-based ML models for
168 predicting other important characteristics like flood depths has not been investigated. Additionally,
169 the importance of spatial distribution of input features has been overlooked in past ML-based flood
170 modeling. To hindcast a flood characteristic at a given location, the features have been
171 incorporated at that location, but flooding is generated through contributions by several other
172 factors that are relevant across the upstream contributing watershed (in inland systems) and/or
173 from the downstream coastline (in coastal systems). The investigation of these research gaps
174 highlighted above is crucial to improve our capability in reliably hindcasting maximum flood
175 depths using computationally efficient and easy-to-use modeling frameworks.

176 This paper aimed to fill these research gaps by examining the performance and transferability
177 of ML models in hindcasting maximum flood depths across various events in a coastal watershed.



178 Our objective was to develop a transferable, computationally efficient model to hindcast flood
179 depths. To achieve this, the study developed a modeling framework based on an ML algorithm.
180 The developed ML-based model combined the ANN algorithm with feature selection methods and
181 geospatial data. We evaluated the performance of this model against one extreme flood event,
182 Hurricane Ida, across a coastal watershed (HUC6)—Lower Hudson—in Northeastern US. Next,
183 we assessed the transferability of our developed model across three other extreme events—
184 Hurricanes Isaias, Sandy, and Irene—in the same watershed. These events encompass varied
185 rainfall intensities, wind speeds and storm track directions. Unlike past ML-based modeling
186 studies, which focused solely on predicting flood status (flooded or unflooded), our regression-
187 based model estimates maximum flood depths. This model was also examined against multiple
188 events, more than one single event that has been the focus of past research (Bafitlhile and Li 2019;
189 Dawson et al. 2006; Hosseini et al. 2020). The model also considered the spatial dimension for
190 predicting flood depths at a given location, in which the features were represented either at that
191 location or across the contributing watershed. This ML model is generic and can be applied to
192 hindcast flood depths at non-gauge river sites to get a denser reconstruction of an event along the
193 river network and hindcast water levels in watersheds with similar drainage area (HUC6 or larger)
194 and flood type (fluvial and coastal).

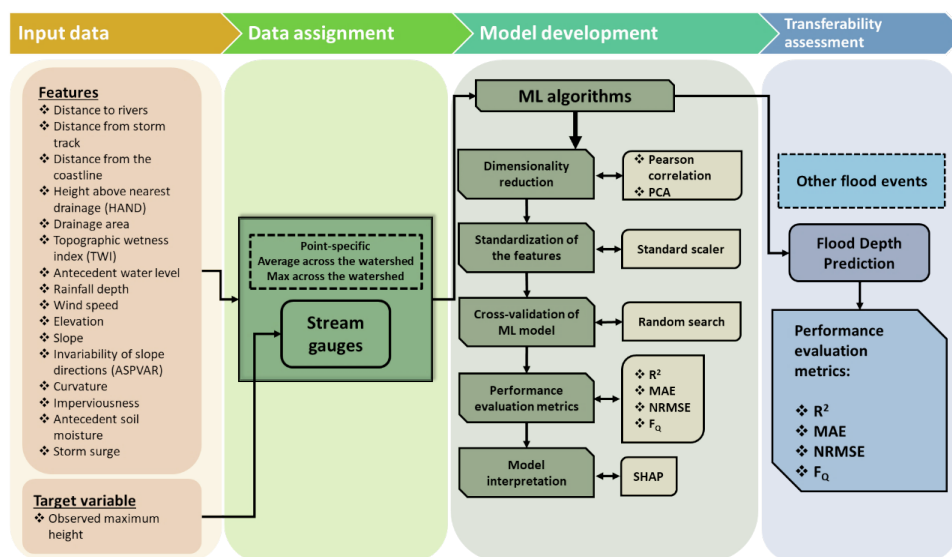
195 **2. Methodology**

196 We developed an ML-based model that hindcast maximum flood depths at stream gauges
197 across a coastal watershed during an event (Figure 1). A coastal watershed receives flood
198 contributions from the inland and coastal systems (i.e., fluvial, and tidal). The model uses
199 geospatial analyses and ML algorithms to hindcast maximum flood depths during an event at river
200 cross-sections of a given watershed. This model is informed by underlying physical flood



201 processes represented by a wide array of features (topographic, meteorologic, hydrologic, land
 202 surface, soil and hydrodynamic).

203 Geospatial operations were conducted to compute the features at stream gauges and/or over
 204 their contributing watersheds (the upstream area that drains water to the gauge) with a careful
 205 consideration of underlying physical processes. We used feature selection techniques to determine
 206 the most key features and used those in our ML model. Applying observed data from stream gauges
 207 during a flood event, the model was trained, cross-validated and tested. We then evaluated the
 208 model transferability by examining its performance in three other extreme flood events.



209
 210 Figure 1: Schematic view of the machine learning (ML)-based model for hindcasting maximum
 211 flood depths in coastal watersheds. ANN: Artificial neural network; PCA: Principal component
 212 analysis; SHAP: Shapley additive explanations; MAE: Mean absolute error; NRMSE:
 213 Normalized root mean square error; F_Q: ratio of estimated over observed maximum flood depth.



214 **2.1. Selection and calculation of key features**

215 When developing an ML model, the features play a pivotal role in determining its performance
216 and estimation capability. By selecting the most relevant and representative features, we empower
217 the model to discern the underlying patterns and relationships within the data more accurately. The
218 ultimate objective is to enable the model to comprehend the complexities associated with flooding,
219 a phenomenon influenced by a myriad of interrelated factors. For an ML estimation accuracy to
220 be transferable for complex physical phenomena of flooding, the selection process should extend
221 beyond merely choosing features based on their individual statistical significance. Instead, it
222 should focus on identifying features that collectively contribute to a holistic representation of the
223 phenomenon. This approach ensures that the ML model can generalize well to unseen data and
224 handle various real-world scenarios effectively. By incorporating this comprehensive set of
225 features, the ML model can capture the nuanced interactions between these features; this enhances
226 the model estimation performance.

227 We selected key features for our ML-based flood model according to the existing research and
228 the underlying physical processes. Our model considers these features from five broad categories
229 of geographic location, hydrologic, topographic, land surface, soil, and hydrodynamic (Table 1).
230 Here, we provide information on how to derive the features to hindcast flood depths during a flood
231 event in a coastal watershed. Aside from the soil category that represents pre-flood conditions
232 (antecedent soil moisture), all other features represent conditions during a flood event.

233



234 Table 1. Machine learning model features and the assignment approaches for stream gauges.

Category	Feature	Point-specific	Spatial average across the contributing watershed	Spatial maximum across the contributing watershed
Geographic location	Distance to rivers		*	
	Distance from storm track	*		
	Distance from the coastline	*		
Hydrologic	Height above nearest drainage (HAND)		*	
	Drainage area	*		
	Flow accumulation	*		
	Topographic wetness index (TWI)	*	*	
	Antecedent water level	*		
Meteorologic	Rainfall depth	*	*	*
	Wind speed	*	*	*
Topographic	Elevation	*		
	Ground slope	*	*	
	Slope aspect	*	*	
	Slope aspect invariability (ASPVAR)		*	
	Curvature	*	*	
Land surface	Imperviousness		*	
Soil	Antecedent soil moisture	*	*	
Hydrodynamic	Storm surge	*	*	

235

236 By integrating all these factors into our methodology, we developed a flood hindcast model
 237 that accounts for key processes in a coastal watershed. We used a two-step process to assign feature
 238 values to a point located on a stream gauge. Depending on the feature, we assigned specified values
 239 to the gauge itself or its contributing watershed to consider the spatial dimension in flood
 240 generation processes. For the contributing watershed, spatial mean, and maximum across the
 241 contributing watershed of a given stream gauge was computed. This method ensures that the
 242 feature values indicate the overall pertinent physical processes occurring at the streams and
 243 upstream watersheds. Table 1 specifies how each feature was used in our model.



244 For features under the geographic location category, we incorporated distance to rivers—
245 critical factor in determining flood risk in numerous studies (Cao et al. 2020; Rafiei-Sardooi et al.
246 2021), storm track—specific to the flood event from (National Hurricane Center 2022)—and
247 distance to the nearest coastline. The proximity of a location to waterbodies, such as rivers or
248 coastlines, directly influences its vulnerability to flooding. Coastal regions are susceptible to storm
249 surges, which occur during tropical storms or hurricanes. Storm surges are massive walls of
250 seawater that get pushed ashore by intense winds. As a result, coastal areas can experience severe
251 flooding. Storm tracks, however, are pathways in the atmosphere along which storms, such as
252 hurricanes, tropical cyclones, or extratropical storms, tend to move. These storms often carry heavy
253 rainfall, intense winds, and storm surges, which can lead to severe flooding in areas they pass over
254 or affect. The distance to storm track and coastline is both considered “Point-specific” as they are
255 specific to individual locations. However, distance to rivers is identical (zero) at these stream
256 gauges, but different in the contributing watersheds, so we calculated the spatial average distance
257 of the contributing watersheds to the rivers.

258 Under the hydrologic category, we employed four variables of HAND, drainage area, flow
259 accumulation, topographic wetness index (TWI), and antecedent water level. HAND represents
260 the elevation of a location relative to the nearest stream. This feature is widely used in flood
261 modeling due to its ability to hindcast flood-prone areas by considering topography and water flow
262 characteristics (Hu and Demir 2021). As its value at the stream gauges is zero, its spatial average
263 across the contributing watershed was considered. The drainage area provides information about
264 potential runoff, while flow accumulation feature helps predict water flow paths during flood
265 events that is previously used by Löwe et al. (2021) and Pham et al. (2021). Both drainage area
266 and flow accumulation values at point of stream gauge (Point-specific) were captured. TWI was



267 calculated using Equation (1) based on the ground slope and drainage area of the contributing
268 watershed (Beven and Kirkby, 1979), and was used by (Gudiyangada Nachappa et al. 2020; Löwe
269 et al. 2021; Pham et al. 2021; Zahura et al. 2020; Zhao et al. 2020).

$$270 \quad TWI = \ln\left(\frac{\alpha}{\tan(\beta)}\right) \quad (1)$$

271 where, α is the upslope contributing area per unit contour length (as known as the specific
272 catchment area), and β is the local slope gradient in radians. Its value was considered for both
273 “Point-specific” and “spatial average across the contributing watershed” to represent the specific
274 location and the overall characteristics of the contributing watershed. The last feature in this
275 category is antecedent water level which refers to the gauge height one day before the event as was
276 considered “Point-specific” for stream gauges.

277 The meteorologic category features were precipitation (Rafiei-Sardooi et al. 2021) and wind
278 speed. Rainfall is the main driving force for floods (Mishra et al. 2022). Storms can bring intense
279 and prolonged rainfall to certain areas. If a storm passes over or near a location, it can result in
280 excessive precipitation, overwhelming local drainage systems and causing flooding in low-lying
281 or poorly drained areas. Wind speed is another key feature that can influence the severity and
282 extent of flooding, especially in the context of hurricanes. Intense winds during storms and
283 hurricanes generate large and powerful waves in the ocean. These waves can exacerbate the impact
284 of storm surges, causing even more coastal flooding as they crash onto the shore and flood areas
285 even farther inland. We obtained daily precipitation and wind speed data for the entire period of
286 flood event from weather stations of the National Oceanic and Atmospheric Administration
287 National Centers for Environmental Information (NOAA’s NCEI 2022). Their maximum values
288 over a flood event were computed at each station. Using point-based precipitation and wind speed



289 data, we then created a spatially distributed rainfall and wind speed dataset by interpolating the
290 maximum values using the Inverse Distance Weighting (IDW) method (Hosseini et al. 2020).
291 Rainfall depth and wind speed are considered for " Point-specific," "spatial average across the
292 contributing watershed," and "spatial maximum across the contributing watershed." These values
293 capture the intensity of the meteorological conditions at individual points and the overall average
294 and maximum values across the watershed.

295 Elevation, ground slope, slope aspect, aspect invariability (ASPVAR), and curvature were
296 features under the topographic category (Cao et al. 2020; Chen et al. 2023; Huang et al. 2022;
297 Khosravi et al. 2018; Rafiei-Sardooi et al. 2021; Sun et al. 2020). DEM with a resolution of 1/3
298 arc-second (~10 m) was acquired from the United States Geological Survey (USGS 2022). To
299 remove any fake depressions, the DEM sinks were filled. Before beginning any hydrological study
300 with DEM data, this is a suggested step that is frequently employed (Khosravi et al. 2018; D. Zhu
301 et al. 2013). Elevation, ground slope, slope aspect, invariability of slope directions (ASPVAR),
302 and curvature all were derived from DEM. Elevation allows us to identify low-lying regions prone
303 to floods and hindcast the flood depths. Ground slope is one of the most key factors in water
304 movement. The slope of the land, also known as the topography or gradient, plays a crucial role in
305 determining the direction and velocity at which water flows across the landscape. On sloped
306 terrain, water flows along the path of least resistance, which is typically downhill. The angle of
307 the slope determines the speed and volume of surface runoff, influencing the potential for flooding.
308 Slope aspect provides insights into surface runoff distribution and flow concentration by indicating
309 the direction that each slope faces affects hydrologic processes (Gudiyangada Nachappa et al.
310 2020; Rafiei-Sardooi et al. 2021). Similar to (Gudiyangada Nachappa et al. 2020), we divided
311 slope aspect into 10 categories: north (0° - 22.5° ; 337.5° - 360°), northeast (22.5° - 67.5°), east (67.5° -



312 112.5°), southeast (112.5°-157.5°), south (157.5°-202.5°), southwest (202.5°-247.5°), west
313 (247.5°-292.5°), northwest (292.5°-337.5°), and flat (0°). ASPVAR values near zero indicate
314 diverse catchment slope aspects, while values approaching 1.0 imply a dominant direction (Wan
315 Jaafar and Han, 2012). This feature provided information about surface runoff distribution and
316 flow concentration by specifying the direction water would flow across the terrain (Dawson et al.
317 2006). Additionally, analyzing the curvature helped us understand how it impacts flood events, as
318 the topographic curvature plays a role in determining the flow of runoff (Khosravi et al. 2018;
319 Pradhan 2009). Elevation is considered "Point-specific", while ground slope, and curvature are
320 considered for both "Point-specific" and "spatial average" across the contributing watershed,"
321 indicating how these topographic features vary throughout the entire watershed. ASPVAR
322 conceptually represents the "spatial average across the contributing watershed," capturing the
323 overall characteristics of watersheds.

324 The land surface category was represented by only one variable, imperviousness. On
325 impervious surfaces, that reduce the ability of soil to absorb rainfall via infiltration, larger volumes
326 of surface runoff are produced and propagated downstream. In fact, impervious surfaces increase
327 both the quantity and velocity of runoff, and this is due to their higher surface smoothness and
328 lower friction to resist water movement. This rapid flow of water can overwhelm natural
329 waterways, increasing the risk of flooding. We used the spatial average of imperviousness across
330 the contributing watershed in the model.

331 Soil category included antecedent soil moisture, which reflects the pre-storm saturation extent,
332 essential for runoff estimates and high moisture flux production from rain-bearing systems
333 (Ahmadisharaf et al. 2016; Jafarzadegan et al. 2023; Mishra et al. 2022). It is calculated over one
334 day before the storm and considered for both "Point-specific" and "spatial average across the



335 contributing watershed." These values indicate the stream gauge surrounding content and its
336 average value over the entire watershed.

337 In the hydrodynamic category, we used storm surge from tidal gauges on the coast. Storm
338 surge was estimated as the difference between the maximum water level and the astronomical tide
339 during a flood event that was downloaded from NOAA ("NOAA Tides & Currents" 2023). This
340 feature is crucial in hindcasting the impact of coastal contributions to flood events. If the flood
341 event does not receive any coastal contributions, this category can be removed from the list of
342 model features. It is considered for both "Point-specific" and "spatial average across the
343 contributing watershed" presenting the stream gauge and its entire watershed tidal condition.

344

345 2.1.1 Feature selection method

346 We employed common feature selection methods, such as Pearson's correlation coefficients
347 (Cao et al., 2020; Chen et al., 2023; Lee et al., 2020) and principal component analysis (PCA) – a
348 widely used technique in many studies (Abdrabo et al., 2023; Chang et al., 2022; Reckien, 2018)
349 to identify most important features for hindcasting flood depths of a given event in a watershed.
350 The PCA components were evaluated based on their absolute values, allowing us to quantify the
351 contribution of each feature to the overall variance. By summing the absolute values across all
352 features, we obtained importance scores for each feature, which enabled us to rank them in
353 descending order. While the Pearson's correlation coefficients are tailored for assessing linear
354 relationships, the PCA captures both linear and non-linear relationships. The strength and direction
355 of linear relationships between the features and flood depth were evaluated using Pearson's
356 correlation coefficient. Through PCA, we determined which principal components in the feature



357 set captured the most variation. These analyses enabled us to narrow down the initial list of the
358 features.

359

360 **2.2. Machine learning (ML) models**

361 2.2.1. Artificial neural networks (ANNs)

362 To hindcast the flood depth, the target variable, we employed ANN. This algorithm was trained
363 via observed flood depths from stream gauges using the key features selected through our feature
364 selection (Section 2.1). The choice of ANN was based on previous successful applications in
365 complex environmental modeling problems (e.g., Adedeji et al., 2022), including flood depth
366 estimations (e.g., Dawson et al., 2006) (Abrahart, Kneale, and See 2004; Bafitlhile and Li 2019;
367 Berkhahn, Fuchs, and Neuweiler 2019; Dawson et al. 2006; Rumelhart, McClelland, and Group
368 1986; J.-J. Zhu, Yang, and Ren 2023). One of the key advantages of using ANN is its capacity for
369 generalization, as highlighted by Maier et al. (2023), allowing the model to perform well on unseen
370 data, making it robust and reliable for real-world flood estimations. Additionally, ANN has been
371 used in flood estimations due to its ability to determine the relationship between rainfall and runoff
372 without relying on specific physical processes, thus addressing the complexities and limitations
373 encountered in hydrologic models (Bafitlhile and Li, 2019). ANNs are computing systems inspired
374 by the biological neural networks that constitute animal brains (Dawson et al., 2006, p. 200;
375 McCulloch and Pitts, 1943). They are designed to simulate the behavior of biological systems
376 composed of "neurons". ANNs are composed of nodes, or "artificial neurons", connected and
377 operate in parallel. Each connection is assigned a weight that represents its relative importance.
378 During the learning phase, the network learns by adjusting these weights based on the input data
379 it is processing (McCulloch and Pitts, 1943). ANNs have also been widely utilized in flood



380 estimations due to their ability to model complex relationships and their tolerance for noisy data.
381 Considering the robustness, accuracy, and proven success of ANN in flood estimation tasks, it was
382 deemed suitable for our flood depth estimations. Here, ANN was implemented using python's
383 Keras library with TensorFlow backend.

384

385 2.2.2. Machine learning (ML) model pre-processing and implementation

386 The observed flood data and features were split into training and testing sets, with 70% to 90%
387 of the data used for training and 10% to 30% for testing (Joseph 2022; Nguyen et al. 2021). The
388 numerical features in the data were standardized using the StandardScaler function from the Scikit-
389 learn library of python. Hyperparameter optimization is a step in improving the performance of
390 ML models. This process involves identifying the optimal hyper-parameter values for ML
391 classifiers. We used the Random Search cross-validation approach (Boulouard et al. 2022; Hashmi
392 2020) to perform hyper-parameter optimization. This approach performs a randomized search on
393 hyperparameters using cross-validation. The hyperparameters we optimized here included the
394 number of layers, units, activation functions, optimizer, regularization rate, batch size, and epochs.
395 The best hyperparameters were selected based on the negative mean squared error. The ANN
396 model was trained using the training data and the best hyperparameters obtained from the
397 optimization process. To prevent overfitting, we used early stopping and model checkpointing
398 during the model training. Early stopping was implemented to stop training when the validation
399 loss stopped improving, and model checkpointing was used to save the model with the lowest
400 validation loss. Cross-validation was performed using a 5-fold cross-validation strategy during the
401 hyperparameter optimization process. This strategy involved splitting the training data into five
402 subsets and training the model five times, each time using a different subset as the validation set.



403 We allocated 90% of the data for training and 10% for testing. While the portion for test is small,
404 the utilization of cross-validation, randomized hyperparameter search, early stopping, and model
405 checkpointing collectively works to construct a model less susceptible to overfitting on a particular
406 test set. This allocation of 10% for testing, combined with these methodologies, is designed to
407 enhance the model's ability to generalize across diverse scenarios.

408

409 2.2.3. Model performance evaluation

410 The performance of the ANN model was evaluated using coefficient of determination (R^2),
411 Mean Absolute Error (MAE), Normalized Root Mean Square Error (NRMSE), and the ratio of
412 estimated over the observed maximum flood depth (F_Q ; Schubert and Sanders 2012). The R^2
413 metric measures the proportion of variance in the dependent variable predictable from the
414 independent variables. The MAE measures the average magnitude of the errors in a set of
415 estimations without considering their direction (i.e., overestimation or underestimation). The
416 NRMSE is a metric that quantifies the normalized average magnitude of the prediction error. It
417 assesses the relative size of the root mean square error (RMSE) by considering the RMSE in
418 relation to the average of the observation. It is commonly used in regression analysis and a smaller
419 NRMSE value indicates a higher level of agreement between the estimated values and the actual
420 observations (Stow et al. 2003; Ahmadisharaf Ebrahim et al. 2019). These metrics were calculated
421 for both training and testing datasets to assess the model performance.

422



423 2.2.4. Model interpretation

424 To interpret the model and understand the contribution of each feature to the estimation, we
425 used SHapley Additive exPlanations (SHAP) that is a game theoretic approach to explain the
426 output of an ML model (Lundberg and Lee, 2017). It connects optimal credit allocation with local
427 explanations using the classic Shapley values from game theory and their related extensions. The
428 SHAP values interpret the impact of having a certain value for a given feature in comparison with
429 the estimations we would make if that feature took some baseline value (Abdollahi and Pradhan,
430 2021). In other words, SHAP estimates how much each feature contributes to the predictive model
431 output for a particular instance. The SHAP results on the feature importance and their impacts on
432 the model estimation can be presented using a plot to visually show the distribution of impacts of
433 each feature on the model output. A positive SHAP value indicates that the feature's presence
434 increases the model output, while a negative SHAP value indicates that it decreases the model
435 output.

436

437 **2.3. Model transferability across flood events**

438 The ML-based model, which was initially developed, trained, and validated based on one flood
439 event, was subsequently examined as is (with no additional parameter tuning) against other events
440 in terms of the performance and generalizability in hindcasting maximum flood depths. By
441 examining our model against different flood events, we aimed to evaluate its effectiveness in
442 hindcasting flood depths across diverse events. This evaluation allowed us to assess the ML
443 model's ability to handle varying flood conditions and its potential for application in different
444 events in the same watershed.

445



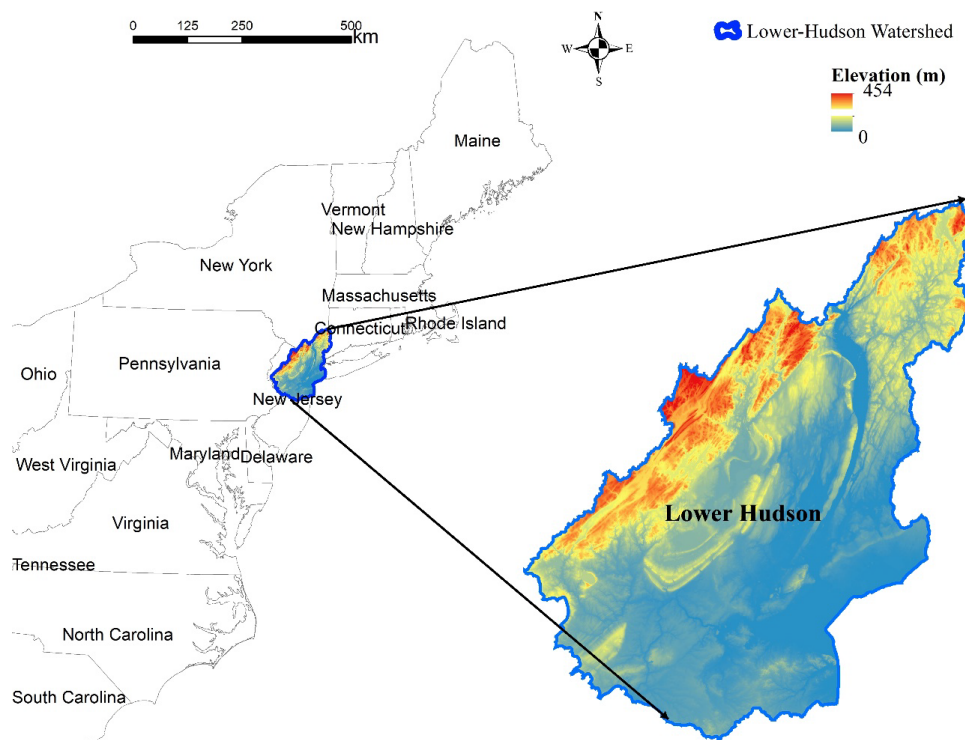
446 **3. Study area**

447 The study area is the Lower Hudson Watershed a six-digit hydrologic unit code (HUC 020301)
448 according to the USGS classification. The 10,068 km² watershed is in the Northeastern United
449 States (Figure 2) spanning parts of three states, Connecticut, New Jersey, and New York. This
450 watershed has a humid subtropical climate with hot summers and mild winters. The highest
451 elevation is ~450 m above mean sea level. Residential, agriculture, and forest are the dominant
452 land uses in the watershed according to the 2022 National Land Cover Dataset (NLCD) (USGS
453 2022). Large metropolitan areas like New York are in the study watershed. The population density
454 was estimated at 344 persons per square km in 2020 (USCB, 2020), with higher concentrations in
455 urban areas like New York and lower densities in rural parts. Several major rivers drain into the
456 watershed, including the Hudson River, which flows for 496 km (about the length of New York
457 State). The ground slope varies from 87.5% in the mountainous parts to 0% in the coastal region.

458 We studied four major flood events in the study area. The primary event for model
459 development was Hurricane Ida in 2021, while three other hurricanes—Isaias (2020), Sandy
460 (2012) and Irene (2011)—were used to assess the model transferability. Hurricane Ida, a
461 devastating Atlantic Category 4 hurricane that made landfall in September 2021, hit Louisiana,
462 and progressed toward the Northeastern United States. The hurricane caused considerable floods
463 and significantly impacted both the west-south-central region, including New Orleans, and the
464 northeastern region, with severe damages reported in New York City and Philadelphia (Beven II,
465 Hagen, and Berg 2022; J. Wang et al. 2022). The storm remnants sent record-breaking rainfall to
466 the New York region as they headed northeast, resulting in flash flooding (Beven II, Hagen, and
467 Berg 2022). The extensive flooding and severe property destruction caused by Hurricane Ida's
468 record-breaking rains highlighted the importance of comprehending the hurricane effects on



469 affected areas. Furthermore, strengthening regional resilience to catastrophic flooding episodes
470 requires the development of effective mitigation strategies. The three other events, which were
471 used to evaluate the model transferability, were also most recent major hurricanes after 2000 with
472 available stream gauge data and differing track and intensity. In 2020, Hurricane Isaias, a Category
473 1 hurricane, made a quick trip along the East Coast, bringing with it severe rain and floods,
474 especially in the Mid-Atlantic and Northeast. The storm's rapid passage caused several deaths and
475 extensive power losses (Latto, Hagen, and Berg 2021). In 2012, superstorm Sandy, commonly
476 known as Hurricane Sandy, struck the Northeast and caused severe damage. It produced significant
477 flooding due to the intense storm surge and torrential rains, especially in New York and New
478 Jersey, where the storm surge reached record heights (Blake et al. 2013). In 2011, a huge and
479 catastrophic storm named Hurricane Irene affected a major portion of the Eastern Seaboard. Heavy
480 rains from the storm caused significant flooding, especially in Vermont, where it was the worst
481 flooding in over a century for that state (Lixion A. and Cangialosi 2013).



482

483

Figure 2. Lower Hudson River Watershed.

484

485 3.1. Data collection

486

487

488

489

490

491

Table 2 lists the data used for the study area alongside their source and spatial and temporal resolutions. We acquired instantaneous stream gauge height data from the USGS's National Water Information System to analyze water levels during the four flood events. While the features' data had different spatial resolutions, we did not make them consistent because only at-point (stream gauges) or aggregated spatial statistics of contributing watersheds were used in the ML model; no combinations of the features were needed.



492 The study watershed embraces 116 stream gauges, seven weather stations and two tidal gauges
 493 (Figure 3). These gauges and stations recorded the data for all the four events (Hurricanes Ida,
 494 Isaias, Sandy, and Irene). The drainage area of the contributing watersheds of the stream gauges
 495 varies from 5.5 to 2,104 km². The range of maximum recorded flood depths, rainfall, and
 496 antecedent soil moisture at the stream gauges during the four hurricanes are presented in Table 2.
 497 It shows that Hurricane Ida had a narrower range of water levels, even though it generated lower
 498 cumulative rainfall depths. In contrast, Hurricane Irene had the broadest range in river water levels,
 499 likely due to the significant amount of rainfall it encountered during the event. Also, Ida and Irene
 500 had similar antecedent soil moisture conditions, which could have influenced their respective river
 501 water levels. Hurricane Sandy had a higher antecedent soil moisture percentage range of 17% to
 502 38% compared to both Ida and Isaias, indicating a potentially higher level of saturation before the
 503 storm's arrival. This may have contributed to Sandy's significant storm surge, which ranged from
 504 1.97 to 2.85 m, compared to Ida and Isaias with storm surge ranges of 0.25 to 0.67 m and 0.20 to
 505 0.76 m, respectively.

506

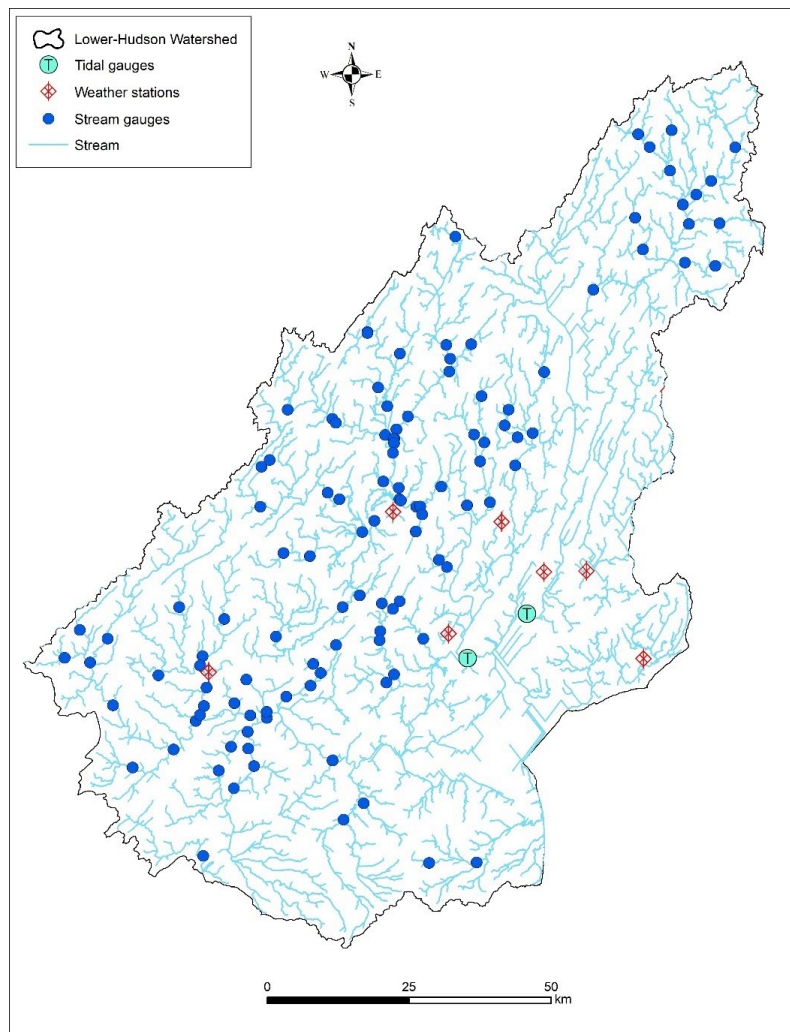
507 Table 2. The range of river water level, cumulative rainfall depth and antecedent soil
 508 moisture in the flood events.

Hurricane	Year	River water level (m)	Cumulative rainfall depth (mm)	Antecedent soil moisture (%)	Storm Surge (m)	Wind Max (m/s)	Distance to storm track (m)
Ida	2021	0.85-36.66	0.01-45.43	21-43%	0.25-0.67	27.64-35.49	0.09-1.1
Isaias	2020	0.22-35.35	17.37-62.22	9-39%	0.20-0.76	48.29-65.33	0.23-1.14
Sandy	2012	0.24-35.98	19.83-56.53	17-38%	1.97-2.85	63.43-76.97	0.77-2.16



Irene	2011	1.03-37.33	147.29-217.74	19-43%	1.05-1.37	51.05-60.68	0.00-0.93
-------	------	------------	---------------	--------	-----------	-------------	-----------

509



510

511

Figure 3. Stream and tidal gauges and weather stations in the study watershed.

512

513

Table 3: Model features and data sources and resolutions in the study area. NHDPlus -

514

National Hydrography Dataset Plus; NED - National Elevation Dataset; USGS NWIS - United

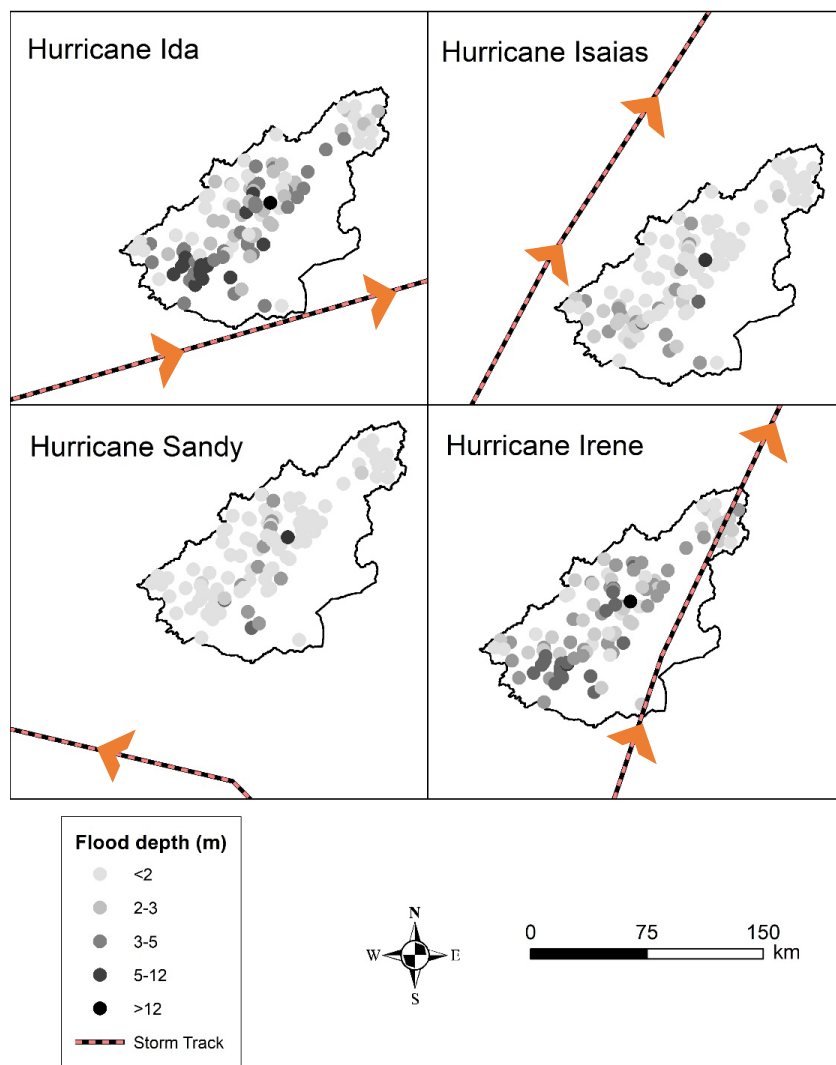


515 States Geological Survey National Water Information System; NCEI - National Centers for
 516 Environmental Information; NLCD - National Land Cover Database; ERA5 - Fifth Generation of
 517 the European Centre for Medium-Range Weather Forecasts (ECMWF) Reanalysis; NOAA -
 518 National Oceanic and Atmospheric Administration.

Category	Feature	Source	Spatial resolution	Temporal resolution
Geographic location	Distance to rivers		—	—
	Distance from storm track	NHDPlus	—	—
	Distance from the coastline		—	—
Hydrologic	Height above nearest drainage (HAND)	NED	10 m	—
	Drainage area		—	—
	Flow accumulation		—	—
	Topographic wetness index (TWI)		—	—
Meteorologic	Rainfall depth	NCEI	—	Daily
	Wind speed			
Topographic	Elevation	NLCD	10 m	—
	Ground slope			—
	Slope aspect invariability (ASPVAR)			—
	Curvature			—
Land surface	Imperviousness	NLCD	30 m	—
Soil	Antecedent soil moisture	ERA5	—	Daily
Hydrodynamic	Storm surge	NOAA Tides and Currents	—	Sub-hourly

519

520 Figure 4 displays the variations in water levels and storm tracks for all hurricanes. The total
 521 slope aspect is south, which results in shallower depths at the upper point of the river. As we
 522 move southward along the river's mainstream, deeper water levels are observed.



523

524

Figure 4. Water levels across the study area during studied hurricanes.



525 **4. Results and discussion**

526 **4.1. Feature selection**

527 4.1.1. Pearson's correlation matrix

528 As a result of Pearson's correlation analyses, we eliminated five features with absolute
529 correlation coefficients greater than 0.70, the cutoff threshold suggested in previous studies (Cao
530 et al. 2020; Chen et al. 2023; Lee et al. 2020). The strong correlation coefficient of 0.99 between
531 "Drainage area" and "Flow accumulation" indicated that both variables capture similar information
532 about water flow and storage in the watershed. To avoid collinearity issues, "Flow accumulation"
533 was excluded from further analyses. Similarly, the high correlation coefficient of 0.97 between
534 "Rain-MAX" and "Rain-Mean" suggested that they offer similar information about maximum and
535 average rainfall values across the watershed. Consequently, "Rain-Mean" was excluded from
536 consideration. Additionally, a correlation coefficient of 0.94 between "Tide-Mean" and "Tide-
537 Point" indicated that the average tide level within the watershed closely resembled tide levels
538 measured at stream gauge points. As a result, "Tide-Point" was excluded from the analysis. By
539 considering the correlation coefficients and the potential redundancy among features, we ensured
540 that independent variables, which are essential for modeling flood depths, are selected.

541 4.1.2. Principal Component Analysis (PCA)

542 We conducted PCA to assess the importance of various features in hindcasting flood depths.
543 The results of the PCA analysis unveiled the key features that significantly influence the flood
544 depth.

545 Interestingly, we identified the "Slope-Point", river slope at the stream gauges, "Slope-
546 Aspect," and distance from the coastline as the least key features for capturing the overall variability



547 of maximum flood depth. Consequently, we excluded it from further analyses. The lesser
548 importance of “Slope-Point” and “Slope-Aspect” may be since river slope is related to bathymetry,
549 which is typically not represented well by DEMs (Bhuyian and Kalyanapu 2020).

550

551 **4.2. Machine learning (ML) model development**

552 4.2.1. Model development and performance evaluation

553 We conducted a thorough hyperparameter optimization process to fine-tune the neural network
554 model for estimating the flood depth of Hurricane Ida. The optimization process involved 500 fits,
555 with each fit considering 100 candidates for each of the five folds in the cross-validation. This
556 helps to ensure that the model's performance is robust and not dependent on a specific
557 training/testing split. As a result, the model became more effective in making estimations on
558 unseen data, as indicated by the enhanced testing performance. Furthermore, the optimization
559 process allowed us to find the best combination of hyperparameters that optimized the model's
560 performance. The best hyperparameters were identified as follows: 50 units, a regularization rate
561 of approximately 0.104, the sgd optimizer, one layer, 600 epochs, a batch size of 8, and the elu
562 activation function. These optimized hyperparameters were then used to train the ANN model and
563 evaluate its performance. This meticulous hyperparameter optimization approach ensured that the
564 model was fine-tuned to achieve the best possible performance for estimating flood depths.

565 The model demonstrated excellent performance on the training dataset, with an R^2 of 0.93,
566 indicating that the model can explain 93% of the variance in the training data. The MAE for the
567 training data was 0.64 m, and NRMSE was 28%, suggesting that the model estimations were
568 satisfactory. On the test dataset, the model achieved an R^2 of 0.87, MAE of 0.87 m, and the
569 NRMSE was 33%. These values also show that the model's performance was satisfactory during

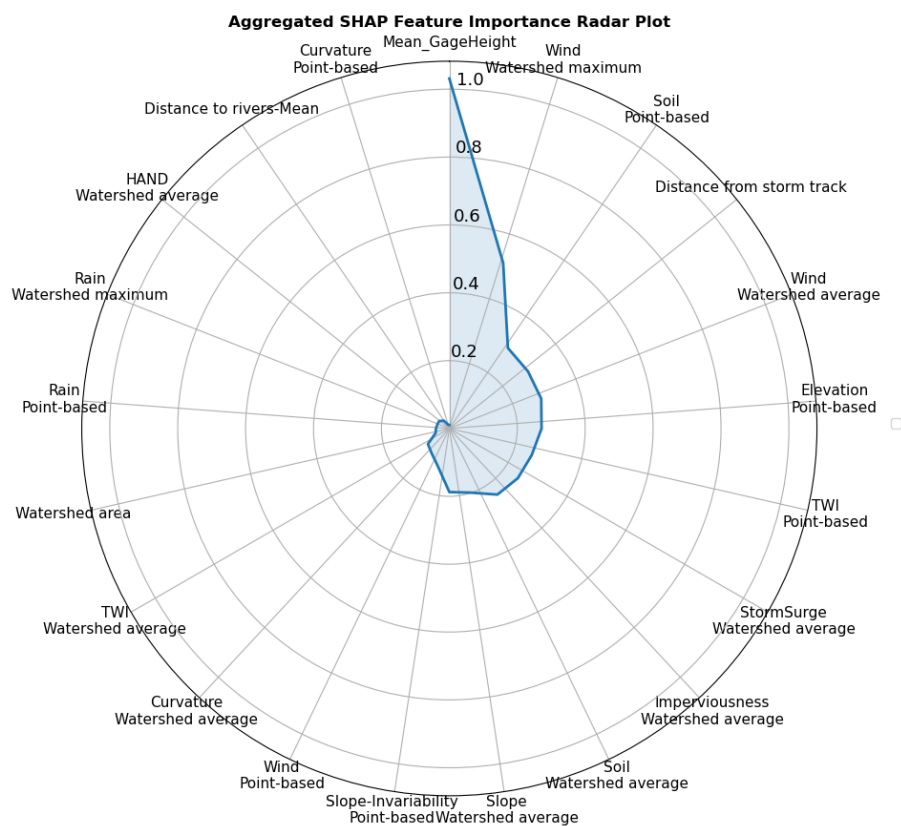


570 the test phase but slightly poorer than the train phase. The training history plot showed that the
571 model performance improved with each epoch during training, indicating that the model was
572 learning from the data. The model training process stopped at epoch 75 due to early stopping.

573

574 4.2.2. Model interpretation

575 Figure 5 provides an overview of the influence of distinctive features on the model estimation
576 on flood depths. The SHAP values measure the contribution of a feature to the estimation for each
577 sample in comparison to the estimation made by a model trained without that feature.



578

579 Figure 5. Shapely additive explanations (SHAP) summary plot of the flood model.



580

581 The most influential features in estimating flood depths are antecedent water level, indicating
582 that streams with higher water levels before an event are subject to greater flood depths. When
583 combined with additional rainfall or water input during a flood, they lead to increased flood depths.
584 Similarly, spatial maximum wind speed across the contributing watershed, antecedent soil
585 moisture at point, and elevation are other significant factors affecting flood depth estimations, with
586 greater values associated with higher estimated flood depths. Intense winds during a hurricane
587 accelerate the movement of floodwaters, leading to greater depths in certain areas, while saturated
588 soil has limited capacity to absorb additional water, resulting in more surface runoff and higher
589 flood depths. The inclusion of elevation as an important feature in our study closely aligns with
590 the findings of Hosseini et al. (2020) and Chen et al. (2023) in their flash flood susceptibility and
591 hazard assessment one on a small non-coastal watershed and the other on a large coastal watershed.
592 Elevation has been consistently recognized as a crucial factor influencing flood occurrences, as it
593 directly affects the water flow and drainage patterns within a watershed (Rafiei-Sardooi et al.
594 2021).

595 On the other hand, features such as the spatial average of distance to rivers across the
596 contributing watershed, the spatial average of HAND across the contributing watershed, and
597 rainfall both at point and the spatial maximum of it across the watershed were identified as the
598 least key features in estimating flood depths. This can be attributed to the fact that our target is
599 hindcasting flood depths at stream gauges, while these input features are more associated with
600 flood depths occurring away from the stream network. Consequently, these features exhibit a
601 limited impact on the model predictive performance when compared to other factors. The spatial
602 average of distance to rivers and HAND have limited variability within our watershed and might



603 not fully capture relevant information about geography, topography, and drainage patterns, leading
604 to reduced discriminatory importance in flood depth estimation models.

605 The finding about the less importance of rainfall in flood estimation concurs with the results
606 reported in the study by Salvati et al. (2023) in pinpointing vulnerable regions within a non-coastal
607 medium-sized watershed. The study suggests that rainfall may have a lower impact on flood
608 occurrences or flood depth estimations compared to other influential factors. This highlights the
609 significance of considering a comprehensive set of variables in flood modeling to accurately
610 capture the underlying relationships and improve estimation performance. The model ability to
611 capture these complex relationships demonstrated its potential utility in flood estimation and
612 management.

613

614 **4.3. Examining the machine learning (ML) model transferability across flood events**

615 The transferability of the trained and tested model (against Hurricane Ida) was examined by
616 applying it to three other events within the same watershed. Table 4 summarizes the evaluation
617 metrics for the three hurricanes.

618

619 Table 4. Model performance across in historical flood events. MAE - mean absolute error;
620 RMSE - root mean square error, F_Q - ratio of estimated over observed maximum flood depth.

Flood event	R^2	MAE (meters)	NRMSE (%)	F_Q (%)
Original Model				
Hurricane Ida	0.92	0.66	29	138
Transferability				
Hurricane Isaias	0.77	1.44	80	322



Hurricane Sandy	0.71	1.69	109	366
Hurricane Irene	0.8	1.19	43	113

621

622 These results demonstrated the model ability to generalize across different hurricanes within the
623 same watershed ($R^2 > 0.71$). With a MAE less than 1.69 m in all hurricanes, our model's
624 performance is consistent with Guo et al. (2021), demonstrating its capability for reasonable flood
625 depth estimates under hurricane conditions. However, when compared to the original model
626 performance on Hurricane Ida, the R^2 values and other metrics show weaker model performance
627 for the transferability to other hurricanes, suggesting reduced estimative accuracy, but not to the
628 extent that the model performance becomes unsatisfactory.

629 Figure 6 presents the flood estimations for all four events. In both Hurricanes Ida and Irene,
630 the model exhibited patterns of overestimation and underestimation across the study watershed.
631 For Hurricanes Isaias and Sandy, we primarily observed overestimations, which may be attributed
632 to their storm track locations. Furthermore, based on Figure 4, we mostly observe overestimation
633 in shallower locations and underestimation for deeper water levels at the stream gauges. This
634 pattern aligns with the southward total slope aspect, where the upper point of the river tends to
635 have shallower depths and the mainstream exhibits deeper water levels.

636 The model achieved an R^2 of 0.80 for Hurricane Irene, scoring 0.77 for Isaias and 0.71 for
637 Sandy. Based on table 2, Hurricanes Ida and Irene exhibited significant similarities in river water
638 levels and antecedent soil moisture. Given that river water level is the target variable and
639 antecedent soil moisture is a crucial feature, better model transferability for Hurricane Irene
640 compared to Hurricanes Isaias and Sandy are expected. The spatial relationship between storm
641 tracks and watershed locations also plays a part in the model performance. Both Hurricanes Ida



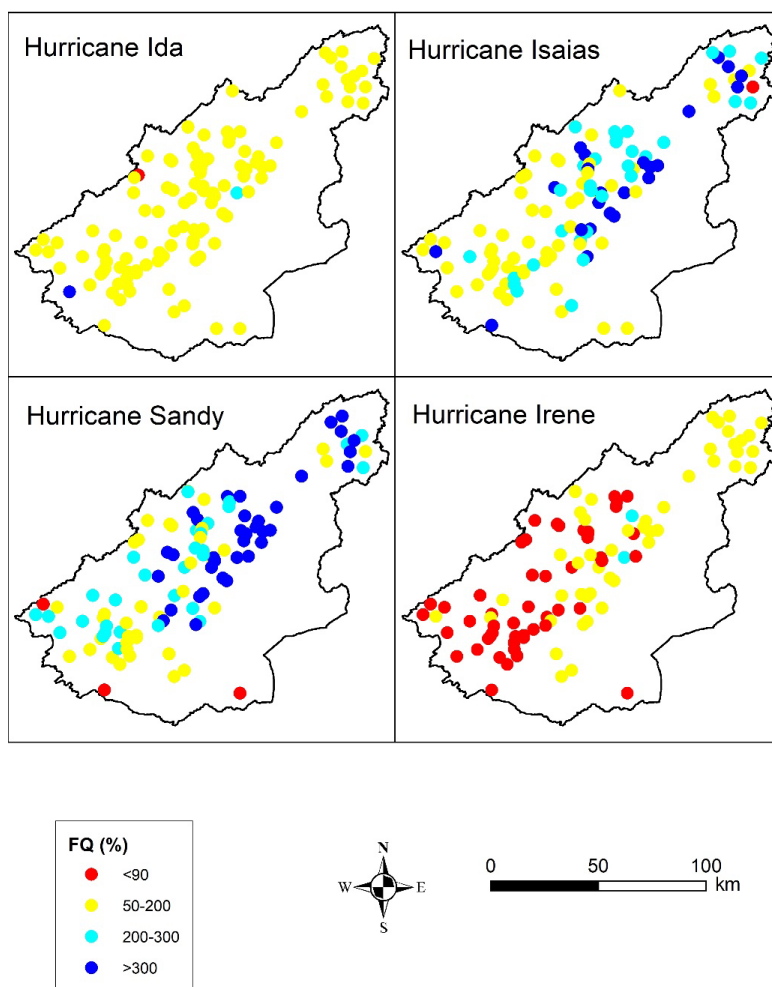
642 and Irene followed similar storm tracks, located on the watershed's eastern side within a
643 comparable distance range. In contrast, Irene tracked were on the west side of the watershed, and
644 Hurricane Sandy was further south from the watershed. The model input feature "distance to storm
645 track" played a significant role, contributing to better transferability to Hurricane Irene due to its
646 similarity with hurricane Ida. However, the ML model still demonstrated satisfactory performance
647 on Hurricane Sandy, suggesting some level of transferability, mainly because we incorporated a
648 wide array of pertinent flood influencing features. This sensitivity underscores the importance of
649 training ML models on diverse hurricane trajectories and proximity to improve the model
650 transferability. While the model performs well, the inconsistency of the success level of
651 transferability across flood events presents opportunities to incorporate additional features or
652 training approaches, enhancing the model robustness to different storm tracks relative to the
653 watershed.

654 The MAE values were higher for Hurricanes Sandy and Isaias, particularly when they were
655 farther away from the storm track. For instance, Hurricane Sandy had the highest MAE (1.69 m)
656 among the transferability cases, indicating larger estimation errors compared to the other
657 hurricanes. The model overestimated flood depths of Hurricanes Sandy and Isaias, while it
658 underestimated those during Hurricane Ida and Irene, likely due to their distance to the storm track.
659 Additionally, hurricanes Sandy and Isaias tend to yield higher F_Q values. For example, Hurricane
660 Sandy had the highest F_Q (366%), indicating larger discrepancies between the estimations and the
661 observed flood depths compared to Hurricanes Irene and Isaias.

662 These findings highlight the challenges of accurately hindcasting flood depths during more
663 severe hurricanes and underscore the importance of further refining the model to enhance its
664 performance in extreme events. Further investigations into the underlying features contributing to



665 these variations are crucial for improving flood hindcast models in the future. Insights gained from
666 this study can help develop transferable ML-based models that are computationally efficient for
667 flood hindcast.



668

669 Figure 6: The ratio of estimated over observed flood depth (F_Q) for the four hurricanes.



670 **4.4. Limitations and future research**

671 While this study showed promising results about ML-based flood modeling, it is important to
672 acknowledge its limitations to identify areas for future research. One significant limitation is the
673 presence of inherent uncertainties in the model that can impact the accuracy of the estimations.
674 These uncertainties can stem from various sources, including the quality and accuracy of the input
675 data (features). For instance, relying solely on spatially aggregated values of features (mean and
676 maximum used in this study) may not adequately capture the complex characteristics of the upper
677 watershed. Future research should prioritize addressing these uncertainties by exploring alternative
678 data sources and methodologies. The ANN model was tuned using observed flood data and a
679 hyperparameter set was used as the optimal parameterization scenario. This deterministic approach
680 does not incorporate the uncertainty from model parameterization. Probabilistic models are needed
681 to address this uncertainty.

682 Furthermore, we did not have sub-daily data available for all our model features. Incorporating
683 sub-daily data can highly likely improve the model accuracy in capturing intra-daily variability
684 and flood dynamics, but it was not explored due to data constraints. Future research should
685 incorporate sub-daily data into flood depth hindcast models. A further limitation of this study
686 related to the time dimension is that wind events, storm surges, rainfall and overland flow
687 processes have different time signatures. Pluvial and storm surge flooding can be closely
688 coincident with the storm event, but river floodwaves may take much longer to arrive at a particular
689 location. The time lag between these processes was not considered in our ML model, which was
690 not dynamic in time and only hindcasted maximum river flood depths. Incorporating time-
691 variability of the features can better represent the time-varying nature of flood dynamics.



692 Another limitation of this study is the issue of bathymetry and the need for further analyses to
693 incorporate better data in coastal watersheds. However, using DEMs without added bathymetry is
694 not entirely inaccurate, as they can already include bathymetry information in regions where
695 LiDAR can penetrate beneath clear water surfaces, particularly in rivers with low suspended
696 sediment and turbidity. On the other hand, coastal floods confined within riverbanks may heavily
697 depend on the main channel slope, while extreme events leading to flooding outside the channel
698 banks follow the general slope of floodplains and this is easily represented by DEMs without
699 considering underwater bathymetry.

700 Additionally, we modeled flood depths across a large watershed (HUC6), whereby many
701 details may not be important. For small watersheds and specially urbanized ones, we emphasize
702 the importance of considering local factors such as sewer and drainage systems in flood depth
703 hindcast, where pluvial floods may be prevalent. However, obtaining comprehensive and accurate
704 data on sewer and drainage systems can be challenging due to availability, lack of quality and
705 confidentiality of the data, particularly at the desired spatial and temporal resolutions. Future
706 research should strive to improve the availability and accessibility of such data to enhance the
707 accuracy and reliability of flood depth hindcasting, especially in urban areas. In small urban
708 watersheds, other details such as land management practices and other local features can also be
709 important for flood depth hindcasting and should be incorporated in the ML-based model.

710 This study primarily focused on hindcasting maximum flood depths and did not consider other
711 important flood characteristics, such as flood duration, frequency, and extent, all of which are
712 important for loss estimates, decision making and risk management (Ahmadisharaf and Kalyanapu
713 2019; Kreibich et al. 2009; Merz et al. 2010; H. Qi and Altinakar 2011b; 2011a; 2012). To gain a
714 fuller picture of flood hazards, future research should aim to develop ML models that can hindcast



715 these additional flood characteristics. We also focused on river flood depths and did not hindcast
716 inundation on floodplains. Developing ML-based models that can satisfactorily hindcast out-of-
717 channel flood depths should be a focus of future research; the transferability of ML-based models
718 for such estimations should be also evaluated. High water marks (HWMs) can be used to train the
719 model for such hindcasting. However, HWMs are subject to large uncertainties (Schubert et al.
720 2022). Therefore, one challenge in developing models that hindcast flood depths over floodplains
721 is the availability of reliable observations. Satellite-based observations are also often limited to
722 flood status data; flood depths cannot be estimated using these types of datasets. Newly launched
723 satellites, such as the Surface Water and Ocean Topography (SWOT) mission, can provide
724 additional data for such estimations.

725 As part of future work, it is also essential to consider the sensitivity of stream gauges to changes
726 in flow once water exceeds bankfull levels. This is significant as water height changes at a slower
727 rate beyond bankfull due to the compound channel shape. Wide floodplains can lead to similar
728 stage elevations for quite different flow conditions. This sensitivity assessment can offer insights
729 about whether water levels can be estimated once flood conditions are established, which has
730 implications for the model transferability across events.

731 We recommend that future work compares the performance of our ML-based model to
732 traditional physically-based and morphologic-based models using the same datasets. By evaluating
733 the performance, generalizability, and computational efficiency of our ML-based model versus
734 these traditional modeling approaches, we will be able to better validate the strengths of our data-
735 driven methodology. Detailed error analyses between the approaches can also reveal insights into
736 where additional physics knowledge needs to be incorporated into the ML-based model structure
737 and training to improve performance.



738 Thus, although we found ML-based models are transferable across flood events when informed
739 by relevant physical features at meaningful locations, there are still several areas that require
740 further investigations. By addressing these limitations, future research can corroborate our findings
741 about the performance and transferability of ML-based models in estimating maximum flood
742 depths as computationally-efficient modeling frameworks.

743 **5. Summary and conclusions**

744 This paper developed an ML-based model for hindcast maximum flood depths to address two
745 major limitations of past research in applying ML models for flood estimations: solely predicting
746 flood status (classification-based models) and debate on the transferability of these models across
747 events. We used ANN to hindcast maximum flood depths over an event on a coastal watershed,
748 which is affected by fluvial and tidal floods. The model was informed by underlying physical flood
749 processes, represented through a set of features (geographic location, topographic, climatic, land
750 surface, hydrologic, hydrodynamic and soil). Unlike previous applications of ML algorithms, our
751 model estimated flood depths by accounting for the spatial distribution of the processes through
752 considering both local contributions (at a given location) and those from the upstream watersheds.
753 We demonstrated the model on a HUC6 watershed, Lower Hudson Watershed, in the Northeastern
754 United States and evaluated its transferability across major flood events—Hurricanes Ida, Sandy,
755 Irene and Isaias. Feature selection techniques were used to identify the most influential features
756 for flood hindcast. Hyperparameter optimization was performed to fine-tune the ML model, and
757 its performance was evaluated using various metrics. The results showed that the model performed
758 satisfactorily in estimating maximum flood depths for the original event, Hurricane Ida ($R^2= 0.92$,
759 MAE= 0.66, NRMSE= 29%, and $F_Q= 139\%$). The model transferability (i.e., applying the
760 validated model as is without any additional parameter tuning) within the same watershed against



761 three other events showed that the developed model was promising in the estimations ($R^2 > 0.71$,
762 $MAE < 1.69$, $NRMSE < 109\%$, and $F_Q < 366\%$). This showed the model ability to capture complex
763 relationships between the maximum flood depth and pertinent features beyond what it was
764 originally trained for. Future research is needed to further evaluate the transferability of ML
765 models across events and watersheds with different drainage areas for flood depth estimations.

766 **Author contribution**

767 **MP:** Data curation, Formal analysis, Investigation, Methodology, Software, Validation,
768 Visualization, Writing – original draft preparation; **EA:** Conceptualization, Methodology, Funding
769 acquisition, Project administration, Supervision, Writing – review & editing; **BN:** Methodology,
770 Writing – review & editing; **EC:** Visualization, Writing – review & editing.

771 **Code availability**

772 The ML codes can be shared upon request.

773 **Data availability**

774 All the data are public domain and can be acquired from online repositories.

775 **Competing interests**

776 The contact author has declared that none of the authors has any competing interests

777 **Acknowledgements**

778 This study was partially supported through a research grant by United States' National Science
779 Foundation (award number 2203180). We thank Paul Bates for the detailed review and fruitful
780 comments on this manuscript.



781 **References**

- 782 Abdollahi, Abolfazl, and Biswajeet Pradhan. 2021. “Urban Vegetation Mapping from Aerial
783 Imagery Using Explainable AI (XAI).” *Sensors* 21 (14): 4738.
784 <https://doi.org/10.3390/s21144738>.
- 785 Abdrabo, Karim I., Sameh A. Kantoush, Aly Esmail, Mohamed Saber, Tetsuya Sumi, Mahmood
786 Almamari, Bahaa Elboshy, and Safaa Ghoniem. 2023. “An Integrated Indicator-Based
787 Approach for Constructing an Urban Flood Vulnerability Index as an Urban Decision-
788 Making Tool Using the PCA and AHP Techniques: A Case Study of Alexandria, Egypt.”
789 *Urban Climate* 48 (March): 101426. <https://doi.org/10.1016/j.uclim.2023.101426>.
- 790 Abraham, Robert, P. E. Kneale, and Linda M. See. 2004. *Neural Networks for Hydrological*
791 *Modeling*. CRC Press.
- 792 Adamowski, Jan, Hiu Fung Chan, Shiv O. Prasher, and Vishwa Nath Sharda. 2011. “Comparison
793 of Multivariate Adaptive Regression Splines with Coupled Wavelet Transform Artificial
794 Neural Networks for Runoff Forecasting in Himalayan Micro-Watersheds with Limited
795 Data.” *Journal of Hydroinformatics* 14 (3): 731–44.
796 <https://doi.org/10.2166/hydro.2011.044>.
- 797 Adedeji, Itunu C., Ebrahim Ahmadisharaf, and Yanshuo Sun. 2022. “Predicting In-Stream Water
798 Quality Constituents at the Watershed Scale Using Machine Learning.” *Journal of*
799 *Contaminant Hydrology* 251 (December): 104078.
800 <https://doi.org/10.1016/j.jconhyd.2022.104078>.
- 801 Ahmadisharaf Ebrahim, Camacho René A., Zhang Harry X., Hantush Mohamed M., and
802 Mohamoud Yusuf M. 2019. “Calibration and Validation of Watershed Models and



- 803 Advances in Uncertainty Analysis in TMDL Studies.” *Journal of Hydrologic Engineering*
804 24 (7): 03119001. [https://doi.org/10.1061/\(ASCE\)HE.1943-5584.0001794](https://doi.org/10.1061/(ASCE)HE.1943-5584.0001794).
- 805 Ahmadisharaf, Ebrahim, and Alfred J Kalyanapu. 2019. “A Coupled Probabilistic Hydrologic and
806 Hydraulic Modelling Framework to Investigate the Uncertainty of Flood Loss Estimates.”
807 *Journal of Flood Risk Management* 12 (S2): e12536. <https://doi.org/10.1111/jfr3.12536>.
- 808 Ahmadisharaf, Ebrahim, Alfred J. Kalyanapu, Brantley A. Thames, and Jason Lillywhite. 2016.
809 “A Probabilistic Framework for Comparison of Dam Breach Parameters and Outflow
810 Hydrograph Generated by Different Empirical Prediction Methods.” *Environmental*
811 *Modelling & Software* 86 (December): 248–63.
812 <https://doi.org/10.1016/j.envsoft.2016.09.022>.
- 813 Anderson, Tiffany R., Charles H. Fletcher, Matthew M. Barbee, Bradley M. Romine, Sam Lemmo,
814 and Jade M. S. Delevaux. 2018. “Modeling Multiple Sea Level Rise Stresses Reveals up
815 to Twice the Land at Risk Compared to Strictly Passive Flooding Methods.” *Scientific*
816 *Reports* 8 (1): 14484. <https://doi.org/10.1038/s41598-018-32658-x>.
- 817 Bafitlhile, Thabo Michael, and Zhijia Li. 2019. “Applicability of ϵ -Support Vector Machine and
818 Artificial Neural Network for Flood Forecasting in Humid, Semi-Humid and Semi-Arid
819 Basins in China.” *Water* 11 (1): 85. <https://doi.org/10.3390/w11010085>.
- 820 Bates, Paul D. 2022. “Flood Inundation Prediction.” *Annual Review of Fluid Mechanics* 54 (1):
821 287–315. <https://doi.org/10.1146/annurev-fluid-030121-113138>.
- 822 Bates, Paul D., Richard J. Dawson, Jim W. Hall, Matthew S. Horritt, Robert J. Nicholls, Jon Wicks,
823 and Mohamed Ahmed Ali Mohamed Hassan. 2005. “Simplified Two-Dimensional
824 Numerical Modelling of Coastal Flooding and Example Applications.” *Coastal*
825 *Engineering* 52 (9): 793–810. <https://doi.org/10.1016/j.coastaleng.2005.06.001>.



- 826 Bentivoglio, Roberto, Elvin Isufi, Sebastian Nicolaas Jonkman, and Riccardo Taormina. 2022.
827 “Deep Learning Methods for Flood Mapping: A Review of Existing Applications and
828 Future Research Directions.” *Hydrology and Earth System Sciences* 26 (16): 4345–78.
829 <https://doi.org/10.5194/hess-26-4345-2022>.
- 830 Berkahn, Simon, Lothar Fuchs, and Insa Neuweiler. 2019. “An Ensemble Neural Network Model
831 for Real-Time Prediction of Urban Floods.” *Journal of Hydrology* 575 (August): 743–54.
832 <https://doi.org/10.1016/j.jhydrol.2019.05.066>.
- 833 Beven II, John L., Andrew Hagen, and Robbie Berg. 2022. “Tropical Cyclone Report -
834 HURRICANE IDA (AL092021).” National Hurricane Center. April 4, 2022.
835 https://www.nhc.noaa.gov/data/tcr/AL092021_Ida.pdf.
- 836 Beven, K. J., and M. J. Kirkby. 1979. “A Physically Based, Variable Contributing Area Model of
837 Basin Hydrology / Un Modèle à Base Physique de Zone d’appel Variable de l’hydrologie
838 Du Bassin Versant.” *Hydrological Sciences Bulletin* 24 (1): 43–69.
839 <https://doi.org/10.1080/02626667909491834>.
- 840 Bhuyian, Md N. M., and Alfred Kalyanapu. 2020. “Predicting Channel Conveyance and
841 Characterizing Planform Using River Bathymetry via Satellite Image Compilation
842 (RiBaSIC) Algorithm for DEM-Based Hydrodynamic Modeling.” *Remote Sensing* 12 (17):
843 2799. <https://doi.org/10.3390/rs12172799>.
- 844 Blake, Eric S., Todd B. Kimberlain, Robert J. Berg, John P. Cangialosi, and John L. Beven II.
845 2013. “Tropical Cyclone Report - Hurricane Sandy (AL182012).” National Hurricane
846 Center. February 12, 2013. https://www.nhc.noaa.gov/data/tcr/AL182012_Sandy.pdf.



- 847 Boulouard, Zakaria, Mariyam Ouaisa, Mariya Ouaisa, Farhan Siddiqui, Mutiq Almutiq, and
848 Moez Krichen. 2022. “An Integrated Artificial Intelligence of Things Environment for
849 River Flood Prevention.” *Sensors* 22 (23): 9485. <https://doi.org/10.3390/s22239485>.
- 850 Cao, Yifan, Hongliang Jia, Junnan Xiong, Weiming Cheng, Kun Li, Quan Pang, and Zhiwei Yong.
851 2020. “Flash Flood Susceptibility Assessment Based on Geodetector, Certainty Factor, and
852 Logistic Regression Analyses in Fujian Province, China.” *ISPRS International Journal of*
853 *Geo-Information* 9 (12): 748. <https://doi.org/10.3390/ijgi9120748>.
- 854 Chang, Li-Chiu, Jia-Yi Liou, and Fi-John Chang. 2022. “Spatial-Temporal Flood Inundation
855 Nowcasts by Fusing Machine Learning Methods and Principal Component Analysis.”
856 *Journal of Hydrology* 612 (September): 128086.
857 <https://doi.org/10.1016/j.jhydrol.2022.128086>.
- 858 Chen, Yuguo, Xinyi Zhang, Kejun Yang, Shiyi Zeng, and Anyu Hong. 2023. “Modeling Rules of
859 Regional Flash Flood Susceptibility Prediction Using Different Machine Learning
860 Models.” *Frontiers in Earth Science* 11.
861 <https://www.frontiersin.org/articles/10.3389/feart.2023.1117004>.
- 862 Costabile, Pierfranco, Carmelina Costanzo, and Francesco Macchione. 2017. “Performances and
863 Limitations of the Diffusive Approximation of the 2-d Shallow Water Equations for Flood
864 Simulation in Urban and Rural Areas.” *Applied Numerical Mathematics*, New Trends in
865 Numerical Analysis: Theory, Methods, Algorithms and Applications (NETNA 2015), 116
866 (June): 141–56. <https://doi.org/10.1016/j.apnum.2016.07.003>.
- 867 Davenport, Frances V., Marshall Burke, and Noah S. Diffenbaugh. 2021. “Contribution of
868 Historical Precipitation Change to US Flood Damages.” *Proceedings of the National*
869 *Academy of Sciences* 118 (4): e2017524118. <https://doi.org/10.1073/pnas.2017524118>.



- 870 Dawson, C. W., R. J. Abrahart, A. Y. Shamseldin, and R. L. Wilby. 2006. “Flood Estimation at
871 Ungauged Sites Using Artificial Neural Networks.” *Journal of Hydrology* 319 (1): 391–
872 409. <https://doi.org/10.1016/j.jhydrol.2005.07.032>.
- 873 Elkharchy, Ismail. 2022. “Flash Flood Water Depth Estimation Using SAR Images, Digital
874 Elevation Models, and Machine Learning Algorithms.” *Remote Sensing* 14 (3): 440.
875 <https://doi.org/10.3390/rs14030440>.
- 876 Fernández-Pato, Javier, Daniel Caviedes-Voullième, and Pilar García-Navarro. 2016.
877 “Rainfall/Runoff Simulation with 2D Full Shallow Water Equations: Sensitivity Analysis
878 and Calibration of Infiltration Parameters.” *Journal of Hydrology* 536 (May): 496–513.
879 <https://doi.org/10.1016/j.jhydrol.2016.03.021>.
- 880 Galloway, Gerald E, Allison Reilly, Sung Ryoo, Anjanette Riley, Maggie Haslam, Sam Brody,
881 Wesley Highfield, Joshua Goldstein, Jayton Rainey, and Sherry Parker,. 2018. “Urban-
882 Flooding-Report-Online.Pdf.” THE GROWING THREAT OF URBAN FLOODING: A
883 NATIONAL CHALLENGE. 2018. [https://today.tamu.edu/wp-](https://today.tamu.edu/wp-content/uploads/sites/4/2018/11/Urban-flooding-report-online.pdf)
884 [content/uploads/sites/4/2018/11/Urban-flooding-report-online.pdf](https://today.tamu.edu/wp-content/uploads/sites/4/2018/11/Urban-flooding-report-online.pdf).
- 885 Gray W. Brunner. 2016. “HEC-RAS, River Analysis System Hydraulic Reference Manual.”
886 February 2016. [https://www.hec.usace.army.mil/software/hec-ras/documentation/HEC-](https://www.hec.usace.army.mil/software/hec-ras/documentation/HEC-RAS%205.0%20Reference%20Manual.pdf)
887 [RAS%205.0%20Reference%20Manual.pdf](https://www.hec.usace.army.mil/software/hec-ras/documentation/HEC-RAS%205.0%20Reference%20Manual.pdf).
- 888 Gudiyangada Nachappa, Thimmaiah, Sepideh Tavakkoli Piralilou, Khalil Gholamnia, Omid
889 Ghorbanzadeh, Omid Rahmati, and Thomas Blaschke. 2020. “Flood Susceptibility
890 Mapping with Machine Learning, Multi-Criteria Decision Analysis and Ensemble Using
891 Dempster Shafer Theory.” *Journal of Hydrology* 590 (November): 125275.
892 <https://doi.org/10.1016/j.jhydrol.2020.125275>.



- 893 Guo, Zifeng, João P. Leitão, Nuno E. Simões, and Vahid Moosavi. 2021. “Data-Driven Flood
894 Emulation: Speeding up Urban Flood Predictions by Deep Convolutional Neural
895 Networks.” *Journal of Flood Risk Management* 14 (1): e12684.
896 <https://doi.org/10.1111/jfr3.12684>.
- 897 Hashmi, Farukh. 2020. “How to Tune Hyperparameters Using Random Search CV in Python.”
898 *Thinking Neuron* (blog). September 10, 2020. [https://thinkingneuron.com/how-to-tune-
899 hyperparameters-using-random-search-cv-in-python/](https://thinkingneuron.com/how-to-tune-hyperparameters-using-random-search-cv-in-python/).
- 900 Hemmati, Mona, Bruce R. Ellingwood, and Hussam N. Mahmoud. 2020. “The Role of Urban
901 Growth in Resilience of Communities Under Flood Risk.” *Earth’s Future* 8 (3).
902 <https://doi.org/10.1029/2019EF001382>.
- 903 Hino, Miyuki, and Earthea Nance. 2021. “Five Ways to Ensure Flood-Risk Research Helps the
904 Most Vulnerable.” *Nature* 595 (7865): 27–29. [https://doi.org/10.1038/d41586-021-01750-
905 0](https://doi.org/10.1038/d41586-021-01750-0).
- 906 Hosseini, Farzaneh Sajedi, Bahram Choubin, Amir Mosavi, Narjes Nabipour, Shahaboddin
907 Shamshirband, Hamid Darabi, and Ali Torabi Haghighi. 2020. “Flash-Flood Hazard
908 Assessment Using Ensembles and Bayesian-Based Machine Learning Models: Application
909 of the Simulated Annealing Feature Selection Method.” *Science of The Total Environment*
910 711 (April): 135161. <https://doi.org/10.1016/j.scitotenv.2019.135161>.
- 911 Hosseiny, Hossein, Foad Nazari, Virginia Smith, and C. Nataraj. 2020. “A Framework for
912 Modeling Flood Depth Using a Hybrid of Hydraulics and Machine Learning.” *Scientific
913 Reports* 10 (1): 8222. <https://doi.org/10.1038/s41598-020-65232-5>.
- 914 Hu, Anson, and Ibrahim Demir. 2021. “Real-Time Flood Mapping on Client-Side Web Systems
915 Using HAND Model.” *Hydrology* 8 (2): 65. <https://doi.org/10.3390/hydrology8020065>.



- 916 Huang, Faming, Siyu Tao, Deying Li, Zhipeng Lian, Filippo Catani, Jinsong Huang, Kailong Li,
917 and Chuhong Zhang. 2022. “Landslide Susceptibility Prediction Considering
918 Neighborhood Characteristics of Landslide Spatial Datasets and Hydrological Slope Units
919 Using Remote Sensing and GIS Technologies.” *Remote Sensing* 14 (18): 4436.
920 <https://doi.org/10.3390/rs14184436>.
- 921 Jafarzadegan, Keighobad, and Venkatesh Merwade. 2019. “Probabilistic Floodplain Mapping
922 Using HAND-Based Statistical Approach.” *Geomorphology* 324 (January): 48–61.
923 <https://doi.org/10.1016/j.geomorph.2018.09.024>.
- 924 Jafarzadegan, Keighobad, Hamid Moradkhani, Florian Pappenberger, Hamed Moftakhari, Paul
925 Bates, Peyman Abbaszadeh, Reza Marsooli, et al. 2023. “Recent Advances and New
926 Frontiers in Riverine and Coastal Flood Modeling.” *Reviews of Geophysics* 61 (2):
927 e2022RG000788. <https://doi.org/10.1029/2022RG000788>.
- 928 Joseph, V. Roshan. 2022. “Optimal Ratio for Data Splitting.” *Statistical Analysis and Data
929 Mining: The ASA Data Science Journal* 15 (4): 531–38.
930 <https://doi.org/10.1002/sam.11583>.
- 931 Kalyanapu, Alfred J., Siddharth Shankar, Eric R. Pardyjak, David R. Judi, and Steven J. Burian.
932 2011. “Assessment of GPU Computational Enhancement to a 2D Flood Model.”
933 *Environmental Modelling & Software* 26 (8): 1009–16.
934 <https://doi.org/10.1016/j.envsoft.2011.02.014>.
- 935 Khosravi, Khabat, Binh Thai Pham, Kamran Chapi, Ataollah Shirzadi, Himan Shahabi, Inge
936 Revhaug, Indra Prakash, and Dieu Tien Bui. 2018. “A Comparative Assessment of
937 Decision Trees Algorithms for Flash Flood Susceptibility Modeling at Haraz Watershed,



- 938 Northern Iran.” *Science of The Total Environment* 627 (June): 744–55.
939 <https://doi.org/10.1016/j.scitotenv.2018.01.266>.
- 940 Kim, Sooyoul, Yoshiharu Matsumi, Shunqi Pan, and Hajime Mase. 2016. “A Real-Time Forecast
941 Model Using Artificial Neural Network for after-Runner Storm Surges on the Tottori
942 Coast, Japan.” *Ocean Engineering* 122 (August): 44–53.
943 <https://doi.org/10.1016/j.oceaneng.2016.06.017>.
- 944 Kratzert, Frederik, Daniel Klotz, Mathew Herrnegger, Alden K. Sampson, Sepp Hochreiter, and
945 Grey S. Nearing. 2019. “Toward Improved Predictions in Ungauged Basins: Exploiting the
946 Power of Machine Learning.” *Water Resources Research* 55 (12): 11344–54.
947 <https://doi.org/10.1029/2019WR026065>.
- 948 Kreibich, H., K. Piroth, I. Seifert, H. Maiwald, U. Kunert, J. Schwarz, B. Merz, and A. H. Thielen.
949 2009. “Is Flow Velocity a Significant Parameter in Flood Damage Modelling?” *Natural
950 Hazards and Earth System Sciences* 9 (5): 1679–92. [https://doi.org/10.5194/nhess-9-1679-](https://doi.org/10.5194/nhess-9-1679-2009)
951 2009.
- 952 Kulp, Scott A., and Benjamin H. Strauss. 2019. “New Elevation Data Triple Estimates of Global
953 Vulnerability to Sea-Level Rise and Coastal Flooding.” *Nature Communications* 10 (1):
954 4844. <https://doi.org/10.1038/s41467-019-12808-z>.
- 955 Kundzewicz, ZW, Buda Su, Yanjun Wang, Jun Xia, Jinlong Huang, and Tong Jiang. 2019. “Flood
956 Risk and Its Reduction in China.” *Advances in Water Resources* 130 (August): 37–45.
957 <https://doi.org/10.1016/j.advwatres.2019.05.020>.
- 958 Latto, Andy, Andrew Hagen, and Robbie Berg. 2021. “Tropical Cyclone Report - HURRICANE
959 ISAIAS (AL092020).” National Hurricane Center. June 11, 2021.
960 https://www.nhc.noaa.gov/data/tcr/AL092020_Isaias.pdf.



- 961 Lee, Deuk-Hwan, Yun-Tae Kim, and Seung-Rae Lee. 2020. “Shallow Landslide Susceptibility
962 Models Based on Artificial Neural Networks Considering the Factor Selection Method and
963 Various Non-Linear Activation Functions.” *Remote Sensing* 12 (7): 1194.
964 <https://doi.org/10.3390/rs12071194>.
- 965 Lixion A., Avila, and John Cangialosi. 2013. “Tropical Cyclone Report - Hurricane Irene
966 (AL092011).” National Hurricane Center. April 11, 2013.
967 https://www.nhc.noaa.gov/data/tcr/AL092011_Irene.pdf.
- 968 Löwe, Roland, Julian Böhm, David Getreuer Jensen, Jorge Leandro, and Søren Højmark
969 Rasmussen. 2021. “U-FLOOD – Topographic Deep Learning for Predicting Urban Pluvial
970 Flood Water Depth.” *Journal of Hydrology* 603 (December): 126898.
971 <https://doi.org/10.1016/j.jhydrol.2021.126898>.
- 972 Lundberg, Scott, and Su-In Lee. 2017. “A Unified Approach to Interpreting Model Predictions.”
973 arXiv. <http://arxiv.org/abs/1705.07874>.
- 974 Maier, Holger R., Stefano Galelli, Saman Razavi, Andrea Castelletti, Andrea Rizzoli, Ioannis N.
975 Athanasiadis, Miquel Sánchez-Marrè, Marco Acutis, Wenyan Wu, and Greer B.
976 Humphrey. 2023. “Exploding the Myths: An Introduction to Artificial Neural Networks
977 for Prediction and Forecasting.” *Environmental Modelling & Software* 167 (September):
978 105776. <https://doi.org/10.1016/j.envsoft.2023.105776>.
- 979 McCulloch, Warren S., and Walter Pitts. 1943. “A Logical Calculus of the Ideas Immanent in
980 Nervous Activity.” *The Bulletin of Mathematical Biophysics* 5 (4): 115–33.
981 <https://doi.org/10.1007/BF02478259>.



- 982 Merz, B, Heidi Kreibich, R Schwarze, and Annette Thielen. 2010. "Review Article" Assessment
983 of Economic Flood Damage".*Natural Hazards and Earth System Sciences* 10: 1697–
984 1724. <https://doi.org/10.5194/nhess-10-1697-2010>.
- 985 Ming, Xiaodong, Qihua Liang, Xilin Xia, Dingmin Li, and Hayley J. Fowler. 2020. "Real-Time
986 Flood Forecasting Based on a High-Performance 2-D Hydrodynamic Model and
987 Numerical Weather Predictions." *Water Resources Research* 56 (7): e2019WR025583.
988 <https://doi.org/10.1029/2019WR025583>.
- 989 Mishra, Ashok, Sourav Mukherjee, Bruno Merz, Vijay P. Singh, Daniel B. Wright, Villarini
990 Gabriele, Subir Paul, et al. 2022. "An Overview of Flood Concepts, Challenges, and Future
991 Directions." *Journal of Hydrologic Engineering* 27 (6).
992 [https://ascelibrary.org/doi/full/10.1061/\(ASCE\)HE.1943-5584.0002164](https://ascelibrary.org/doi/full/10.1061/(ASCE)HE.1943-5584.0002164).
- 993 Mosavi, Amir, Pinar Ozturk, and Kwok-wing Chau. 2018. "Flood Prediction Using Machine
994 Learning Models: Literature Review." *Water* 10 (11): 1536.
995 <https://doi.org/10.3390/w10111536>.
- 996 National Academies of Sciences, Engineering, and Medicine. 2019. *Framing the Challenge of*
997 *Urban Flooding in the United States*. Washington, DC: The National Academies Press.
998 <https://doi.org/10.17226/25381>.
- 999 National Hurricane Center. 2022. "National Hurricane Center." 2022.
1000 <https://www.nhc.noaa.gov/index.shtml>.
- 1001 Nguyen, Quang Hung, Hai-Bang Ly, Lanh Si Ho, Nadhir Al-Ansari, Hiep Van Le, Van Quan Tran,
1002 Indra Prakash, and Binh Thai Pham. 2021. "Influence of Data Splitting on Performance of
1003 Machine Learning Models in Prediction of Shear Strength of Soil." *Mathematical*



- 1004 *Problems in Engineering* 2021 (February): e4832864.
1005 <https://doi.org/10.1155/2021/4832864>.
- 1006 “NOAA Tides & Currents.” 2023. CO-OPS Map - NOAA Tides & Currents. 2023.
1007 <https://tidesandcurrents.noaa.gov/map/index.html>.
- 1008 NOAA’s NCEI. 2022. “Data Search | National Centers for Environmental Information (NCEI).”
1009 2022. <https://www.ncei.noaa.gov/access/search/data-search/local-climatological-data>.
- 1010 Pham, Binh Thai, Chinh Luu, Tran Van Phong, Phan Trong Trinh, Ataollah Shirzadi, Somayeh
1011 Renoud, Shahrokh Asadi, Hiep Van Le, Jason von Meding, and John J. Clague. 2021. “Can
1012 Deep Learning Algorithms Outperform Benchmark Machine Learning Algorithms in
1013 Flood Susceptibility Modeling?” *Journal of Hydrology* 592 (January): 125615.
1014 <https://doi.org/10.1016/j.jhydrol.2020.125615>.
- 1015 Pradhan, Biswajeet. 2009. “Journal of Spatial Hydrology Vol.9, No.2 Fall 2009.”
- 1016 Qi, Honghai, and Mustafa S. Altinakar. 2011a. “A Conceptual Framework of Agricultural Land
1017 Use Planning with BMP for Integrated Watershed Management.” *Journal of*
1018 *Environmental Management* 92 (1): 149–55.
1019 <https://doi.org/10.1016/j.jenvman.2010.08.023>.
- 1020 ———. 2011b. “Vegetation Buffer Strips Design Using an Optimization Approach for Non-Point
1021 Source Pollutant Control of an Agricultural Watershed.” *Water Resources Management* 25
1022 (2): 565–78. <https://doi.org/10.1007/s11269-010-9714-9>.
- 1023 ———. 2012. “GIS-Based Decision Support System for Dam Break Flood Management under
1024 Uncertainty with Two-Dimensional Numerical Simulations.” *Journal of Water Resources*
1025 *Planning and Management* 138 (4): 334–41. [https://doi.org/10.1061/\(ASCE\)WR.1943-](https://doi.org/10.1061/(ASCE)WR.1943-5452.0000192)
1026 5452.0000192.



- 1027 Qi, Wenchao, Chao Ma, Hongshi Xu, Zifan Chen, Kai Zhao, and Hao Han. 2021. “A Review on
1028 Applications of Urban Flood Models in Flood Mitigation Strategies.” *Natural Hazards* 108
1029 (1): 31–62. <https://doi.org/10.1007/s11069-021-04715-8>.
- 1030 Rafiei-Sardooi, Elham, Ali Azareh, Bahram Choubin, Amir H. Mosavi, and John J. Clague. 2021.
1031 “Evaluating Urban Flood Risk Using Hybrid Method of TOPSIS and Machine Learning.”
1032 *International Journal of Disaster Risk Reduction* 66 (December): 102614.
1033 <https://doi.org/10.1016/j.ijdr.2021.102614>.
- 1034 Rahmati, Omid, Hamid Reza Pourghasemi, and Hossein Zeinivand. 2016. “Flood Susceptibility
1035 Mapping Using Frequency Ratio and Weights-of-Evidence Models in the Golastan
1036 Province, Iran.” *Geocarto International* 31 (1): 42–70.
1037 <https://doi.org/10.1080/10106049.2015.1041559>.
- 1038 Reckien, Diana. 2018. “What Is in an Index? Construction Method, Data Metric, and Weighting
1039 Scheme Determine the Outcome of Composite Social Vulnerability Indices in New York
1040 City.” *Regional Environmental Change* 18 (5): 1439–51. [https://doi.org/10.1007/s10113-](https://doi.org/10.1007/s10113-017-1273-7)
1041 [017-1273-7](https://doi.org/10.1007/s10113-017-1273-7).
- 1042 Rennó, Camilo Daleles, Antonio Donato Nobre, Luz Adriana Cuartas, João Viane Soares, Martin
1043 G. Hodnett, Javier Tomasella, and Maarten J. Waterloo. 2008. “HAND, a New Terrain
1044 Descriptor Using SRTM-DEM: Mapping Terra-Firme Rainforest Environments in
1045 Amazonia.” *Remote Sensing of Environment* 112 (9): 3469–81.
1046 <https://doi.org/10.1016/j.rse.2008.03.018>.
- 1047 Rezaie, Fatemeh, Mahdi Panahi, Sayed M. Bateni, Changhyun Jun, Christopher M. U. Neale, and
1048 Saro Lee. 2022. “Novel Hybrid Models by Coupling Support Vector Regression (SVR)



- 1049 with Meta-Heuristic Algorithms (WOA and GWO) for Flood Susceptibility Mapping.”
1050 *Natural Hazards* 114 (2): 1247–83. <https://doi.org/10.1007/s11069-022-05424-6>.
- 1051 Rumelhart, David E., James L. McClelland, and PDP Research Group. 1986. *Parallel Distributed*
1052 *Processing: Explorations in the Microstructure of Cognition: Foundations*. The MIT
1053 Press. <https://doi.org/10.7551/mitpress/5236.001.0001>.
- 1054 Salvati, Aryan, Alireza Moghaddam Nia, Ali Salajegheh, Kayvan Ghaderi, Dawood Talebpour
1055 Asl, Nadhir Al-Ansari, Feridon Solaimani, and John J. Clague. 2023. “Flood Susceptibility
1056 Mapping Using Support Vector Regression and Hyper-Parameter Optimization.” *Journal*
1057 *of Flood Risk Management* n/a (n/a): e12920. <https://doi.org/10.1111/jfr3.12920>.
- 1058 Schubert, Jochen E., Adam Luke, Amir AghaKouchak, and Brett F. Sanders. 2022. “A Framework
1059 for Mechanistic Flood Inundation Forecasting at the Metropolitan Scale.” *Water Resources*
1060 *Research* 58 (10): e2021WR031279. <https://doi.org/10.1029/2021WR031279>.
- 1061 Schubert, Jochen E., and Brett F. Sanders. 2012. “Building Treatments for Urban Flood Inundation
1062 Models and Implications for Predictive Skill and Modeling Efficiency.” *Advances in Water*
1063 *Resources* 41 (June): 49–64. <https://doi.org/10.1016/j.advwatres.2012.02.012>.
- 1064 Sridhar, Venkataramana, Syed Azhar Ali, and David J. Sample. 2021. “Systems Analysis of
1065 Coupled Natural and Human Processes in the Mekong River Basin.” *Hydrology* 8 (3): 140.
1066 <https://doi.org/10.3390/hydrology8030140>.
- 1067 Stow, Craig A., Chris Roessler, Mark E. Borsuk, James D. Bowen, and Kenneth H. Reckhow.
1068 2003. “Comparison of Estuarine Water Quality Models for Total Maximum Daily Load
1069 Development in Neuse River Estuary.” *Journal of Water Resources Planning and*
1070 *Management* 129 (4): 307–14. [https://doi.org/10.1061/\(ASCE\)0733-](https://doi.org/10.1061/(ASCE)0733-9496(2003)129:4(307))
1071 [9496\(2003\)129:4\(307\)](https://doi.org/10.1061/(ASCE)0733-9496(2003)129:4(307)).



- 1072 Sun, Deliang, Jiahui Xu, Haijia Wen, and Yue Wang. 2020. “An Optimized Random Forest Model
1073 and Its Generalization Ability in Landslide Susceptibility Mapping: Application in Two
1074 Areas of Three Gorges Reservoir, China.” *Journal of Earth Science* 31 (6): 1068–86.
1075 <https://doi.org/10.1007/s12583-020-1072-9>.
- 1076 USGS. 2022. “TNM Download V2.” 2022. <https://apps.nationalmap.gov/downloader/>.
- 1077 Viglione, Alberto, Giuliano Di Baldassarre, Luigia Brandimarte, Linda Kuil, Gemma Carr, José
1078 Luis Salinas, Anna Scolobig, and Günter Blöschl. 2014. “Insights from Socio-Hydrology
1079 Modelling on Dealing with Flood Risk – Roles of Collective Memory, Risk-Taking
1080 Attitude and Trust.” *Journal of Hydrology*, Creating Partnerships Between Hydrology and
1081 Social Science: A Priority for Progress, 518 (October): 71–82.
1082 <https://doi.org/10.1016/j.jhydrol.2014.01.018>.
- 1083 Wan Jaafar, Wan Zurina, and Dawei Han. 2012. “Uncertainty in Index Flood Modelling Due to
1084 Calibration Data Sizes.” *Hydrological Processes* 26 (2): 189–201.
1085 <https://doi.org/10.1002/hyp.8135>.
- 1086 Wang, Jie, Qiuhong Tang, Xiaobo Yun, Aifang Chen, Siao Sun, and Dai Yamazaki. 2022. “Flood
1087 Inundation in the Lancang-Mekong River Basin: Assessing the Role of Summer
1088 Monsoon.” *Journal of Hydrology* 612 (September): 128075.
1089 <https://doi.org/10.1016/j.jhydrol.2022.128075>.
- 1090 Wang, Zhaoli, Chengguang Lai, Xiaohong Chen, Bing Yang, Shiwei Zhao, and Xiaoyan Bai.
1091 2015. “Flood Hazard Risk Assessment Model Based on Random Forest.” *Journal of*
1092 *Hydrology* 527 (August): 1130–41. <https://doi.org/10.1016/j.jhydrol.2015.06.008>.
- 1093 Wing, Oliver E. J., William Lehman, Paul D. Bates, Christopher C. Sampson, Niall Quinn, Andrew
1094 M. Smith, Jeffrey C. Neal, Jeremy R. Porter, and Carolyn Kousky. 2022. “Inequitable



- 1095 Patterns of US Flood Risk in the Anthropocene.” *Nature Climate Change* 12 (2): 156–62.
1096 <https://doi.org/10.1038/s41558-021-01265-6>.
- 1097 Youssef, Ahmed M., Biswajeet Pradhan, Abhirup Dikshit, and Ali M. Mahdi. 2022. “Comparative
1098 Study of Convolutional Neural Network (CNN) and Support Vector Machine (SVM) for
1099 Flood Susceptibility Mapping: A Case Study at Ras Gharib, Red Sea, Egypt.” *Geocarto
1100 International* 37 (26): 11088–115. <https://doi.org/10.1080/10106049.2022.2046866>.
- 1101 Zahura, Faria T., Jonathan L. Goodall, Jeffrey M. Sadler, Yawen Shen, Mohamed M. Morsy, and
1102 Madhur Behl. 2020. “Training Machine Learning Surrogate Models From a High-Fidelity
1103 Physics-Based Model: Application for Real-Time Street-Scale Flood Prediction in an
1104 Urban Coastal Community.” *Water Resources Research* 56 (10).
1105 <https://doi.org/10.1029/2019WR027038>.
- 1106 Zhang, Fang, Xiaolin Zhu, and Desheng Liu. 2014. “Blending MODIS and Landsat Images for
1107 Urban Flood Mapping.” *International Journal of Remote Sensing* 35 (9): 3237–53.
1108 <https://doi.org/10.1080/01431161.2014.903351>.
- 1109 Zhao, Gang, Bo Pang, Zongxue Xu, Lizhuang Cui, Jingjing Wang, Depeng Zuo, and Dingzhi
1110 Peng. 2021. “Improving Urban Flood Susceptibility Mapping Using Transfer Learning.”
1111 *Journal of Hydrology* 602 (November): 126777.
1112 <https://doi.org/10.1016/j.jhydrol.2021.126777>.
- 1113 Zhao, Gang, Bo Pang, Zongxue Xu, Dingzhi Peng, and Depeng Zuo. 2020. “Urban Flood
1114 Susceptibility Assessment Based on Convolutional Neural Networks.” *Journal of
1115 Hydrology* 590 (November): 125235. <https://doi.org/10.1016/j.jhydrol.2020.125235>.
- 1116 Zheng, Xing, David G. Tarboton, David R. Maidment, Yan Y. Liu, and Paola Passalacqua. 2018.
1117 “River Channel Geometry and Rating Curve Estimation Using Height above the Nearest



- 1118 Drainage.” *JAWRA Journal of the American Water Resources Association* 54 (4): 785–
1119 806. <https://doi.org/10.1111/1752-1688.12661>.
- 1120 Zhu, D., Q. Ren, Y. Xuan, Y. Chen, and I. D. Cluckie. 2013. “An Effective Depression Filling
1121 Algorithm for DEM-Based 2-D Surface Flow Modelling.” *Hydrology and Earth System
1122 Sciences* 17 (2): 495–505. <https://doi.org/10.5194/hess-17-495-2013>.
- 1123 Zhu, Jun-Jie, Meiqi Yang, and Zhiyong Jason Ren. 2023. “Machine Learning in Environmental
1124 Research: Common Pitfalls and Best Practices.” *Environmental Science & Technology*,
1125 June. <https://doi.org/10.1021/acs.est.3c00026>.
- 1126